Fan Noise Source Diagnostic Test— LDV Measured Flow Field Results

Gary G. Podboy, Martin J. Krupar, Christopher E. Hughes, and Richard P. Woodward
Glenn Research Center, Cleveland, Ohio

The NASA STI Program Office . . . in Profile

Since its founding, NASA has been dedicated to the advancement of aeronautics and space science. The NASA Scientific and Technical Information (STI) Program Office plays a key part in helping NASA maintain this important role.

The NASA STI Program Office is operated by Langley Research Center, the Lead Center for NASA's scientific and technical information. The NASA STI Program Office provides access to the NASA STI Database, the largest collection of aeronautical and space science STI in the world. The Program Office is also NASA's institutional mechanism for disseminating the results of its research and development activities. These results are published by NASA in the NASA STI Report Series, which includes the following report types:
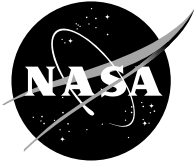
- TECHNICAL PUBLICATION. Reports of completed research or a major significant phase of research that present the results of NASA programs and include extensive data or theoretical analysis. Includes compilations of significant scientific and technical data and information deemed to be of continuing reference value. NASA's counterpart of peer-reviewed formal professional papers but has less stringent limitations on manuscript length and extent of graphic presentations.

- TECHNICAL MEMORANDUM. Scientific and technical findings that are preliminary or of specialized interest, e.g., quick release reports, working papers, and bibliographies that contain minimal annotation. Does not contain extensive analysis.

- CONTRACTOR REPORT. Scientific and technical findings by NASA-sponsored contractors and grantees.

- CONFERENCE PUBLICATION. Collected papers from scientific and technical conferences, symposia, seminars, or other meetings sponsored or cosponsored by NASA.

- SPECIAL PUBLICATION. Scientific, technical, or historical information from NASA programs, projects, and missions, often concerned with subjects having substantial public interest.

- TECHNICAL TRANSLATION. English-language translations of foreign scientific and technical material pertinent to NASA's mission.

Specialized services that complement the STI Program Office's diverse offerings include creating custom thesauri, building customized databases, organizing and publishing research results . . . even providing videos.

For more information about the NASA STI Program Office, see the following:

- Access the NASA STI Program Home Page at *http://www.sti.nasa.gov*

- E-mail your question via the Internet to help@sti.nasa.gov

- Fax your question to the NASA Access Help Desk at 301–621–0134

- Telephone the NASA Access Help Desk at 301–621–0390

- Write to:
  NASA Access Help Desk
  NASA Center for AeroSpace Information
  7121 Standard Drive
  Hanover, MD 21076

Fan Noise Source Diagnostic Test— LDV Measured Flow Field Results

Gary G. Podboy, Martin J. Krupar, Christopher E. Hughes, and Richard P. Woodward
Glenn Research Center, Cleveland, Ohio

National Aeronautics and
Space Administration

Glenn Research Center

Acknowledgments

Fan Noise Source Diagnostic Test—LDV Measured Flow Field Results

Gary G. Podboy,* Martin J. Krupar,+ Christopher E. Hughes,* and Richard P. Woodward*
National Aeronautics and Space Administration
Glenn Research Center
Cleveland, Ohio 44135

Abstract

Results are presented of an experiment conducted to investigate potential sources of noise in the flow developed by two 22-in. diameter turbofan models. The R4 and M5 rotors that were tested were designed to operate at nominal take-off speeds of 12,657 and 14,064 RPMC, respectively. Both fans were tested with a common set of swept stators installed downstream of the rotors. Detailed measurements of the flows generated by the two rotors were made using a laser Doppler velocimeter system. The wake flows generated by the two rotors are illustrated through a series of contour plots. These show that the two wake flows are quite different, especially in the tip region. These data are used to explain some of the differences in the rotor/stator interaction noise generated by the two fan stages. In addition to these wake data, measurements were also made in the R4 rotor blade passages. These results illustrate the tip flow development within the blade passages, its migration downstream, and (at high rotor speeds) its merging with the blade wake of the adjacent (following) blade. Data also depict the variation of this tip flow with tip clearance. Data obtained within the rotor blade passages at high rotational speeds illustrate the variation of the mean shock position across the different blade passages.

Introduction

From 1994 through 2001, The Advanced Subsonic Technology (AST) Noise Reduction Program was conducted by NASA in partnership with the FAA, and U.S. aerospace companies for the purpose of reducing aircraft noise. This program involved two parallel efforts; one aimed at reducing airframe noise, the other focused on reducing engine noise. The goal of the engine noise studies was to reduce engine source noise by 6 EPNdB (Effective Perceived Noise dB) by the year 2000 relative to 1992 technology.

During the AST program numerous experimental tests were conducted to quantify the effectiveness of engine noise reduction concepts. The concepts tested included low-noise fan designs, swept and/or leaned stators, active noise control, fan flow management (trailing edge blowing), and scarfed inlets. A review of this work is provided in ref. 1. Studies of the acoustics of high-bypass ratio turbofans normally divide the engine into four regions: the core, the turbine, the fan, and the jet. Of these, the fan is responsible for creating a major portion of the noise developed by the engine when operating near airports at take-off and approach conditions. Therefore, many of the concepts studied under the AST program have focused on reducing fan noise.

One of the last experimental tests of the AST program was carried out, in part, to identify and characterize noise sources within the fan stage of a turbofan model. This test, conducted at the NASA Glenn 9 X 15 Foot Wind Tunnel in 1999-2000 using a 22-inch (55.9 cm) diameter turbofan model, is known as the Source Diagnostic Test (SDT). The overall test had many phases, including aerodynamic and acoustic performance testing of two different fans and three different stator designs, acoustic mode measurements using sensors located on the inner surface of the duct, spinning mode measurements using a rotating rake in both the inlet and the nozzle, unsteady surface pressure measurements on a set of stator vanes, and detailed flow field diagnostic measurements using laser Doppler and hot-wire anemometry.

The detailed flow field measurements made during the Source Diagnostic Test were obtained in order to get a better understanding of the relationship between the flow within the fan stage and the fan noise produced by the test model. Nonuniformities in the flow field within the fan duct can produce noise when they interact with the solid surfaces within the model. These flow field nonuniformities can be sources of either tone or broadband noise. Periodic nonuniformities in the mean flow created by the spinning rotor blades generate noise at discrete frequencies (tone noise), while the random fluctuations in the flow (turbulence) produce broadband noise. For high-bypass ratio engines, both the tone and broadband noise can be significant contributors to the overall level of fan noise. Consequently, to understand how the fan noise is produced, it is important to get a better understanding of both the periodic and random flow field nonuniformities.

There are a number of potential noise sources in the fan flow. The viscous blade wakes and tip vortices shed from the rotor blades can be important contributors to the noise produced by the fan stage. These wakes and vortices can contain both strong perturbations of the mean flow and high levels of turbulence. The noise produced when these disturbances convect downstream and interact with the stator vanes is known as rotor/stator interaction noise. When operating at high rotational speeds, shocks can form on the rotor blades. These shocks can represent strong, periodic perturbations in the flow. The noise generated by the shocks is known as multiple pure tone or buzzsaw noise. Since broadband noise is generated by the turbulence in the flow, any "source" of turbulence is also a possible source of broadband noise. The turbulence in the rotor flow field is highest in the boundary layers along the hub, case, and blade surfaces and in the viscous wakes and tip vortices shed from the rotor.

There have been a number of previous experimental investigations aimed at characterizing the flow field nonuniformities which produce fan noise. Martens, et. al. (ref. 2) made measurements both upstream and downstream of the stators inside a 22-inch diameter fan model using hot-wire anemometry in an effort to correlate flow characteristics with noise measurements. Ganz (ref. 3) also used hot-wire anemometry to obtain inlet boundary layer and

---

wake flow data inside an 18-inch diameter turbofan model. Podboy (ref. 4) compared the wake flow generated by a fan designed by the Allison Engine Co. with a fan designed by Pratt & Whitney. These studies reveal that the flow field features which are responsible for the generation of fan noise change significantly with RPM, tip clearance, and fan loading. They also suggest that there can be appreciable differences in the fan wake flows generated by different rotors. They imply, therefore, that in order to understand how a particular fan generates noise, it is necessary to either measure the flow experimentally, or to use Computational Fluid Dynamics to identify the flow field features responsible for the noise.

During the Source Diagnostic Test detailed measurements were obtained on the flows generated by two rotors, the R4 and M5. The R4 rotor was designed to operate at 12,657 RPMC; the M5 rotor was designed to operate at 14,064 RPMC (10% higher than the R4 design speed). These two rotors were designed to generate the same overall fan pressure ratio at their respective design speeds. The purpose of testing both rotors was to determine if there was an acoustic advantage of one design relative to the other. Wake flow field measurements were obtained with the two rotors operating at similar operating conditions so that any differences in the rotor/stator interaction noise could be related to differences in the flows generated by the two fans. Both the flow field and far-field acoustic data obtained on each rotor were acquired with a common set of stator vanes installed downstream of the rotors. Thus the only variable in the tested configurations was the rotor. This was important since any differences in the acoustics could then be related directly to the differences in the rotors and the flows which they generate.

The purpose of this paper is to present much of flow field data acquired on the R4 and M5 rotors during the Source Diagnostic Test. As mentioned above, wake data were acquired downstream of the two rotors so that differences in the rotor/stator interaction noise generated by the two fan stages could be related to differences in the wake flows. The wake data acquired for this purpose were obtained at two axial locations downstream of the rotors and at two operating conditions, approach and take-off. Besides this wake data, additional measurements of the R4 rotor flow field were also made. These include R4 rotor wake measurements made at two other operating conditions, below-approach (50% of the design speed) and cut-back (87.5% of the design speed), and measurements made within the R4 rotor blade passages. These intrablade measurements were made for several reasons: 1) to determine how the tip flows generated by the rotor blades develop within the blade passages; 2) to determine how the tip flow development varies with rotor speed, and 3) to characterize the shocks which develop on the R4 blades when they are operated at high speed. All of the data acquired for these purposes are included in this report. These data were obtained with a laser Doppler velocimeter system; some single-point hot-wire measurements of the R4 rotor flow field were included in an earlier report (ref. 5).

Experimental Apparatus and Procedure

Test Model

Figure 1 shows the 22-inch (55.9 cm) diameter turbofan model installed in the test section of the NASA Glenn 9 X 15 Foot Wind Tunnel. Two different rotors, designated as R4 and M5 by the manufacturer (General Electric), were tested during the flow field diagnostic portion of the test. The R4 rotor was designed to operate at 12,657 RPMC; the M5 rotor was designed to operate at 14,064 RPMC. Although they were designed to generate the same overall fan pressure ratio

at their respective design speeds, the experimentally determined value for the M5 rotor was slightly higher than that of the R4 (1.50 vs 1.47). Table 1 shows some additional design parameters of these two rotors.

Table 1. R4 / M5 Fan Design Parameters	
Number of blades	22
Tip diameter, in.	22
Fan hub/tip radius ratio	0.30
Corrected tip speed , ft/s	1,215 / 1,350
Corrected RPM (RPMC)	12,657 / 14,064
Corrected fan weight flow (lbm/s)[*]	100.5 / 102.1
Stage total pressure ratio[*]	1.47 / 1.50
[*] R4 value based on previous test data	

The LDV data were acquired with the same set of stator vanes installed downstream of the two rotors. This stator set had 26 vanes, each having 30 degrees of radial sweep along its leading edge.

It is important to note that the two rotors were thought to have different tip clearances when tested at similar operating conditions. Most of the flow diagnostic testing done on the R4 rotor was conducted with a rubstrip installed within the model which was designed to provide a clearance of 0.020" between the tip of the rotor and the outer case when the rotor was operated at 100% of its design speed. In contrast, the M5 flow field data were acquired with what was called a "nominal" rubstrip installed; this rubstrip was designed so that the M5 blades would contact the rubstrip when the rotor was operated at 100% of its design speed, thus providing no clearance between the fan and the case at this speed. Consequently, at a given operating condition the M5 tip clearance is thought to have been smaller than that of the R4 rotor. The actual tip clearances, however, were not measured during the test. Plans have been made to measure the tip clearances during the next wind tunnel test involving these two rotors.

The flow diagnostic studies were conducted with an inlet different than that shown in the photograph of figure 1. The inlet shown in the photo is similar to that which would be used on a full-scale engine during an actual flight. The LDV data were acquired with a bellmouth inlet installed on the model. The bellmouth inlet provided essentially the same flow into the fan as the flight inlet, but allowed the tunnel to be run at a lower speed. This provided the following benefits: 1) the test was conducted at a lower cost and 2) the LDV system components which were mounted in the test section were subjected to lighter air loads. The test section Mach number during the LDV testing was approximately 0.05.

Laser Velocimeter System and Data Acquisition

Figure 2 shows the locations at which LDV measurements were made relative to the model hardware. Part a) of the figure shows the locations at which data were acquired during testing of the M5 rotor; part b) shows measurement locations for the R4 rotor. Measurements were made downstream of the M5 rotor at two axial locations between the rotor and stator, corresponding to 3.09 and 6.46 inches downstream of the non-rotating position of the M5 tip trailing edge. These two axial locations will be referred to as axial stations LDV1 and LDV2. As shown in the schematic, LDV1 is upstream of LDV2. Data were acquired within these two axial planes with the M5 rotor operating at two different speeds, 8,507 and 14,064 RPMC (60.8 and 100% of the design speed); these speeds correspond to nominal approach and take-off conditions, respectively, for this fan stage. The survey locations shown for the R4 rotor in part b) of the figure are designated as being either wake, tip flow, or shock location

surveys. Wake measurements were made downstream of the R4 rotor at the same two axial locations within the model as the M5 surveys. The LDV1 and LDV2 stations are 3.12 and 6.49 inches, respectively, downstream of the non-rotating position of the tip trailing edge of the R4 rotor. With this rotor, wake data were acquired at four corrected rotor speeds, 6,329, 7,808, 11,074, and 12,657 (50, 61.7, 87.5 and 100% of the design speed). The 7,808, 11,074, and 12,657 speeds correspond to nominal approach, cut-back, and take-off conditions for the R4 fan. The wake surveys made downstream of these two fans were conducted to determine how the wake flows vary with rotor speed and axial location. In addition to these wake measurements, data were also acquired in the tip region of the R4 rotor. The blue vertical lines shown in the blade tip region in part b) of the figure show locations at which data were acquired to determine how the tip flow develops within the R4 rotor blade passages. At these locations data were acquired at 7,808, 11,074, and 12,657 RPMC. The green horizontal line shown in part b) of the figure shows locations at which measurements were made to determine the character of the shocks which form on the R4 blades when this rotor is operated at high speeds. These shock location surveys were made with the rotor operating at 11,074 and 12,657 RPMC.

In order to conduct these LDV surveys it was necessary to place part of the LDV system inside the test section of the wind tunnel. Figure 3 shows a photograph of the LDV traverse system located on the side of the turbofan model. In this photo the bellmouth inlet is shown installed on the model. The traverse was used to move the LDV probe volume radially and axially relative to the model. The LDV system optics are located behind the cylindrical shield shown in the photo. This shield was installed to keep the tunnel flow from striking the optics.

Figure 4 shows a photograph taken with the cylindrical shield removed. In this photo the fiber optic cables used to deliver the laser beams into the tunnel, the transmitting optics used to direct the beams into the model, and one set of receiving optics can be seen. The LDV system is a four-beam, two-color, backscatter system which allows the measurement of two components of velocity simultaneously. Two green beams were used to measure the axial component of velocity, while two blue beams allowed the measurement of tangential component. The photo provided in figure 4 shows one of two optical arrangements used during the test. Initially, another optical arrangement, one employing two sets of receiving optics (one above and one below the transmitting optics) was used to conduct the wake surveys. During these surveys it was possible to measure both the axial and tangential velocity components simultaneously. Later in the test, however, when the intrablade surveys were attempted on the R4 rotor, it was found that the reflection of the laser beams off of the rotor blades were drowning out the LDV signals, making it impossible to acquire data using the optical arrangement employed during the wake surveys. To get data within the blade passages it was necessary to position the receiving optics so that they could not "see" the reflection of the beams off of the blades. Since the laser beams were reflecting off the bottom surface of the blades (the pressure surface), it was necessary to position the receiving optics so that they could not see the bottom surface. This requirement meant that the receiving optics had to be positioned at a relatively large angle above the transmitting optics. This arrangement is shown in the photograph of figure 4. The size of the optical breadboard allowed only one set of receiving optics to be positioned in this way, therefore only one component of velocity could be acquired at a time. Both components of velocity were measured during the intrablade surveys, but they were measured at different times.

Two windows installed in the side of the model permitted optical access to the internal flow. These two windows are shown in the photograph of figure 5. The upstream window shown at the right was used during the shock location and tip flow surveys, while the downstream window shown at the left was used to acquire the wake surveys. These windows, made of 0.1 in. thick sodium alumino silicate, were slumped in a furnace (process given in ref. 6) to have the same shape as the inner contour of the model.

The tunnel flow was seeded with polystyrene latex (PSL) spheres that were manufactured at the NASA Glenn Research Center. Figure 6 shows a photograph taken using a scanning electron microscope of a sample of the PSL particles. The white line in the figure corresponds to a length of one micron. Based on this photo, the nominal size of the PSL spheres is estimated to be approximately 0.7 micron in diameter. As a result of how they are made, the solid PSL particles come from the manufacturer suspended in water. Before introduction into the wind tunnel this solution is diluted by mixing it with 190 proof ethanol. This diluted solution is then sprayed into the tunnel using a set of nine spray nozzles located approximately 80 feet upstream of the test section. The liquid evaporates in the time it takes to reach the test section, leaving behind the solid PSL seed on which the LDV data was obtained.

The individual velocity measurements were sorted into circumferential bins around the rotor using shaft angle encoders fed with the once-per-revolution signal of the rotor. These encoders segmented the 360 degrees of rotor revolution occurring between two consecutive once-per-revolution pulses into 1100 bins of equal width (50 bins per blade passage). Each time a velocity measurement was made, the encoder output was sampled to determine the number of bins generated since the occurrence of the previous once-per-rev pulse. The velocity and corresponding bin number were then stored in the computer as a data pair.

Data were acquired at each measurement location over many rotor revolutions until either a preset number of measurements had been acquired on one of the two LDV channels, or until the maximum time allotted for the data acquisition had elapsed. On-line data plots were used to determine the number of measurements required to accurately resolve the flows occurring within the individual blade passages. In general, the higher the unsteadiness in the flow, the greater the number of measurements required to resolve the flow. On average, more than 40,000 velocity measurements per component were obtained at each combination of measurement location and operating condition.

LDV Data Reduction

Figure 7 illustrates the data reduction process for a velocity component measured at a given location within the model. The top plot (part a) shows raw, unaveraged velocities sorted into the 1100 bins of a rotor revolution. The first step in the data reduction process is to simply find the average of the velocities occurring within each of the 1100 bins. The resulting mean velocity profile across the entire rotor rev is shown in part b) of figure 7. The next step is to compute the standard deviation (rms) with respect to the mean of the velocities occurring within each bin. This standard deviation, which is a measure of the unsteadiness of the velocity component, will be referred to as the turbulent velocity. Figure 7c shows the resulting turbulent velocity distribution. As can be seen from these plots of the mean and turbulent velocity, there is a high degree of similarity between the flows in the individual blade passages. Consequently, little information would be lost in averaging the data of the 22

blade passages into one average passage. The process of computing average passage distributions from the data is illustrated in figure 7d for the mean velocities, and in 7e for the turbulent velocities. This step involves folding the mean and turbulent (rms) velocity data of the 22 individual blade passages into one passage and computing the mean within each bin. Velocity distributions which span the 50 bins of a single passage result from this process. A final step in the data reduction is to compute a circumferentially-averaged mean and turbulent velocity from the average passage distributions. The circumferentially-averaged mean velocity is found by determining the mean of the 50 average passage mean velocities, while the circumferentially-averaged turbulent velocity is the mean of the 50 average passage turbulent velocities.

Results

Wake Surveys

LDV data were obtained in the wake of both the R4 and M5 rotors in order to obtain a better understanding of the flow field nonuniformities which contribute to the rotor/stator interaction noise produced by these fan stages. The viscous blade wakes and tip vortices are the main contributors to this rotor/stator interaction noise. Periodic variations in the mean flow generate discrete tones, while random fluctuations in the flow contribute to the broadband noise. The noise is produced when the wake flow nonuniformities convect downstream and interact with the stator vanes.

Mean Wake Flow: R4 & M5 Rotors

Figure 8 shows an example of mean flow velocities measured in the wake of a rotor using the LDV system. These data were acquired at axial station LDV1 downstream of the R4 rotor with the rotor operating at 100% speed. Both components of velocity measured with the LDV are presented; the upper plot shows average passage axial mean velocities, while the bottom plot shows average passage tangential mean velocities. The view provided in these plots is from downstream of the rotor, looking upstream. The contours depict average passage results, with the average passage data duplicated circumferentially to provide a better view of any transitions which occur across the boundaries of the passage. In this downstream-looking-upstream view, the rotor blades would rotate clockwise. The axial mean velocities shown in the top plot are typical of all such plots made from the wake data obtained during this test in that they clearly identify two distinct regions in the flow: 1) a viscous region made up of both the blade wakes and the outer endwall flow where (as will be shown later) the flow is turbulent, and 2) a potential flow region between adjacent blade wakes and inboard of the endwall flow where the axial velocities are relatively uniform and (also shown later) the flow is steady. In general, at a given radius, axial velocities are lower and tangential velocities higher in the viscous part of the flow.

Any nonuniformities occurring in the circumferential direction in the mean rotor wake flow at the point in time when the wake flow impacts the stators will cause the lift on the stators to vary. This periodic variation in the lift can generate rotor/stator interaction tone noise. Therefore, from an acoustics standpoint, it is of interest to identify the magnitude of these nonuniformities. Figure 9 shows the data of figure 8 replotted to illustrate more clearly the nonuniformities in the mean flow downstream of the R4 rotor. The plotted contour levels were calculated by subtracting, at each radial location, the circumferentially-averaged mean velocity from the average passage mean velocities. As such, the contours depict the oscillation of the mean flow about the

circumferentially-averaged velocity measured at a given radius. The term "perturbation" will be used to describe the magnitude of this oscillation at a given radial location (ie. the maximum minus minimum contour value plotted at a radial location). At this 100% speed condition the mean axial velocity perturbations are highest in the blade wake regions, while the mean tangential velocity perturbations are highest in the tip region. Of these two components, the perturbations in the tangential velocities are thought to be more directly related to the generation of the unsteady lift on the stators. Consequently, the oscillations of the tangential component are thought to be more important to the generation of rotor/stator interaction tone noise.

Figure 10 shows contours of this same parameter (the difference between the average passage mean velocities and the circumferentially-averaged mean velocity measured at each radius) computed from the tangential velocities measured downstream of both the R4 and the M5 rotors at axial station LDV1. Parts a) through d) of the figure show results corresponding to the R4 rotor operating at 50% (part a), 61.7% (approach, part b), 87.5% (cut-back, part c) and 100% speed (take-off, part d); while parts e) and f) show results for the M5 rotor operating at 60.8% (approach, part e) and 100% speed (take-off, part f). Since R4 rotor results are presented at four different speeds, these data can be used to determine how the relative importance of the two primary sources of tone noise in the R4 wake flow, the viscous blade wakes and the tip flows, change with rotor speed. The R4 data show that: 1) at low speed the perturbation of the mean flow caused by the blade wake is higher than the perturbation caused by tip flow; 2) in the blade wake region (inboard of the tip) the perturbation increases steadily up to 87.5% speed, then appears to level off as speed is increased further to 100%; 3) the perturbation in the tip region increases all the way up to 100% speed, and 4) at 100% speed, the tip flow region provides more of a perturbation than the blade wake region.

The results plotted in figure 10 can also be used to determine the amount of similarity in the flows generated by the two rotors at this axial location. A comparison of parts b) and e) of the figure reveals that at the approach condition there are significant differences in the flows, especially at the outer radial locations near the case. One difference is in the wake widths: the M5 rotor wakes are thicker than those of the R4 rotor. The thicker M5 blade wakes result in a smoothly-varying wake flow circumferentially, while the thinner R4 wakes produce higher velocity gradients at the edges of the blade wakes. Due to this difference, the R4 stage would be expected to generate stronger acoustic tones at multiples of the blade passing frequency (BPF). Another difference in the wakes is related to their shapes: although leaned, the M5 rotor wakes are relatively straight; in contrast, the R4 wakes are curved. The curvature in the R4 wakes occurs rather abruptly at about 75% span, producing two distinct segments of the wake: an inboard segment that is leaned much like the M5 wake, and an outboard segment that has very little lean (ie. is radial). A third difference is related to the magnitude of the mean flow perturbation generated in the tip region close to the outer endwall: it is much higher downstream of the M5 rotor at this part speed condition.

A comparison of the plots presented for the take-off condition (100% speed, parts d and f of figure 10) reveals that the two rotor wake flows are similar in that they both show a distinct tip flow "bulging" from the side of the viscous blade wake. For both rotors, this tip flow region represents that part of the blade span which produces the largest perturbation in the mean tangential flow. The main difference in the flows generated by the two rotors at this speed is in the shape of the blade wakes at the outer radial locations: as in the

lower-speed, approach-condition data, the M5 wakes are skewed such that they curve in a direction opposite to the rotation of the rotor (they skew in the counter-clockwise direction); in contrast, the R4 wakes are much more radial.

Figure 11 shows this same parameter plotted for the downstream axial location, LDV2. Note that the colorbar used in this figure has a range (max minus min) less than half of that used in the presentation of the upstream station LDV1 data. This indicates that the perturbations in the mean tangential flow downstream of both rotors are dissipating rapidly as the flows move downstream, making the mean flows more uniform. At the approach condition (61.7% speed for R4 and 60.8% speed for M5) the magnitude of the perturbations generated downstream of the two rotors are roughly the same at all spanwise locations. This was not the case at axial station LDV1. At the upstream axial station the perturbations were similar over the inner 75% of the blade span, but in the tip region the M5 wake flow showed a much higher perturbation. The fact that the difference in the perturbations generated by the two rotors seems to disappear by the time the flows reach station LDV2, suggests that the perturbation generated by the tip of the M5 rotor is dissipating more rapidly than that generated by the R4 rotor. Once again, the most noticeable difference in the wake flows generated by the two rotors at the approach condition involves the shape of the wakes. The differences in the lean of the blade wakes of the two rotors noted in the discussion of the upstream data are even more pronounced at this downstream location. The data are showing that the M5 blade wakes get more skewed as they move downstream. The lean of the M5 wakes, which increases with increasing radius, is in the opposite direction to the rotation of the rotor. In contrast, over the outer 20% of span, the R4 wakes are slanted slightly in the direction of rotor rotation.

The faster rate of decay of the mean tangential velocity perturbation occurring at the approach operating condition in the tip region downstream of the M5 rotor relative to that of the R4 rotor may be related to the differences in the orientation of the blade wakes of the two rotors at the outer radial locations. As noted above, the M5 wakes get skewed as they move downstream, resulting in a great deal of lean in the wakes at the downstream location, especially in the tip region. The tip regions of the R4 blade wakes are much more radial. Consequently, the tip regions of the M5 blade wakes get stretched significantly, whereas the tip regions of the R4 wakes do not. A study by Brookfield et. al. (ref. 7) has shown that stretching tends to reduce the wake velocity deficit associated with a wake. Since the mean axial velocity perturbation (the wake deficit) is reduced by stretching, it seems reasonable to expect that the mean tangential velocity perturbation would also be reduced. If it is true that stretching tends to "even out" the nonuniformities in the mean flow, then the perturbations in the tip region of the M5 rotor would be expected to continue to decay more rapidly than those of the R4 rotor as the two flows move downstream from station LDV2. Consequently, at the stator leading edge location the mean wake flow of the M5 rotor would be more uniform than that of the R4 rotor, and the rotor/stator interaction tone noise produced by the M5 fan stage would be expected to be less than that produced by the R4 stage. In addition, there are two other reasons why the M5 wakes could be expected to generate less tone noise: 1) The skewed M5 wakes result in more rotor blade wakes intersecting a given stator vane at a given point in time. This leads to a phase cancellation effect which is thought to result in reductions of tone noise (ref. 8). 2) The intersection of the blade wakes with the tip regions of the stator vanes would be more orthogonal with the M5 wakes. This tends to minimize the speed of the wake intersection point along the stator leading

edge which, in turn, is also thought to reduce the tone noise (ref. 9). These three factors working in combination can be expected to be responsible for a significant rotor/stator interaction tone noise reduction of the M5 stage relative to the R4 stage at the approach condition.

A comparison of the plots presented in figure 11 for the downstream measurement location, LDV2, at the 100% speed condition (parts d and f) indicates that there are also considerable differences in the wake flows generated by the two rotors at this speed. Recall that in the 100% speed data presented for station LDV1 (figure 10 parts d and f), there were strong disturbances in the mean tangential velocity flows of both rotors at the locations where the tip flows merged with the blade wakes. While it is possible to still identify such a disturbance in the 100% speed, station LDV2 data of the R4 rotor (figure 11 part d), it is not possible to locate such a strong disturbance in the M5 wake data acquired at this speed and axial location (figure 11 part f). It may be that the large amount of stretching of the M5 wake that occurs in the tip region is responsible for making the M5 wake flow more uniform in this region. Based on the differences in the wake flows measured at this speed and axial location, the M5 stage would be expected to produce less rotor/stator interaction tone noise than the R4 stage.

The above mean wake flow results suggest that the M5 stage would be expected to generate less rotor/stator interaction tone noise than the R4 stage at both of the operating conditions at which LDV data were acquired on the two rotors, approach and take-off. Experiments performed to determine the far-field noise levels generated by these fans were conducted in a manner which allows the estimation of the tone noise levels resulting from rotor wake/stator interaction. During this acoustic testing, far-field noise data were acquired both with and without a barrier wall in place next to the model. This allowed two sets of far-field data to be acquired: 1) runs conducted without the barrier wall measured the sum of both the forward and aft-propagating noise (the total noise); 2) runs conducted with the wall in place measured the forward-propagating noise. Subtracting the forward-propagating noise from the total noise allows the determination of the aft-propagating noise. The primary source of the tones in this aft-propagating noise is expected to be the interaction between the nonuniformities in the mean rotor wake flow and the stator vanes. Thus, the expected differences in the rotor/stator interaction tone levels caused by the differences in the mean wake flows of the two rotors should be evident in the aft-propagating tone noise data.

Figure 12 shows plots of the 1BPF, 2BPF, and 3BPF tone power levels generated by both the R4 (in red) and M5 (black) fan stages at speeds ranging from below approach to above take-off. These results correspond to the same rotor/stator configurations tested during the LDV studies (ie. the swept stators were installed). The upper plot (part a) shows forward-propagating tones; the bottom plot (part b) shows aft-propagating tones. As can be seen in the bottom plot, these acoustic results do show the expected lower interaction tone levels for the M5 rotor at the approach condition. Both the 1BPF and 2BPF tones of the M5 stage are over 10 dB lower than those of the R4 stage at this condition. At 100% speed, both stages generate about the same level of the 1BPF tone, while the 2BPF and 3BPF tone levels generated by the M5 stage are about 2 dB and 5dB, respectively, below those generated by the R4 stage. Thus, both the low and high-speed acoustic results show that the M5 stage generates less rotor/stator interaction tone noise than the R4 stage, as expected based on the differences in the mean wake flows generated by the two rotors.

Unsteady Wake Flow: R4 & M5 Rotors

While rotor/stator interaction tone noise can be related to the amplitude and phase of the mean flow variations in the rotor wake flow, rotor/stator interaction broadband noise is a function of the turbulence level in the wake flow. Figure 13 shows an example of turbulent velocities measured downstream of the R4 rotor. These plots depict the turbulent flow corresponding to the mean flow which was presented in figure 8; that is, they show results of measurements made downstream of the R4 rotor at axial station LDV1 with the rotor operating at 100% speed. The upper plot shows contours of average passage axial turbulent velocity; the bottom plot shows average passage tangential turbulent velocity. These clearly show the demarcation between the viscous and potential flow regions of the wake flow. The viscous regions are unsteady, while the potential flow regions between the wakes and inboard of the tip flow are not. A comparison of the two plots indicates that the turbulent velocity contours corresponding to the two components are very similar. As was the case with tone noise, of the two components of velocity measured, the fluctuations of the tangential component are thought to be the more important contributors to the generation of the broadband noise.

Figure 14 shows contours of average passage tangential turbulent velocities measured downstream of both the R4 and the M5 rotors at axial station LDV1. The contours corresponding to the two rotors show a number of similarities: 1) the turbulent regions tend to get thinner as the rotor speeds are increased; 2) the turbulent velocities increase in magnitude with rotor speed, and 3) this increase tends to occur more rapidly in the tip region than in the blade wake. The plots also show that at similar operating conditions the two rotors generate comparable peak levels of tangential turbulent velocity.

The contours plotted in figure 14 also show that there are a number of differences in the wake flows generated by the two rotors. Of the two conditions, approach and take-off, at which data were acquired with both rotors, the differences are more noticeable at approach. At this low-speed condition, there are two major differences in the wake flows: 1) the aforementioned thicker wakes of the M5 rotor, and 2) a significant difference in the shape of the turbulent flows generated by the tips of the two rotors. As can be seen in parts a) and b) of figure 14, a thick region of unsteady flow extends completely across the passage downstream of the tips of the R4 blades when this rotor is operated at low speed. In contrast, the low-speed contours plotted for the M5 rotor (part e of the figure) indicate that the flow in the tip region of this rotor is much less turbulent. In fact, it is not possible to clearly identify a separate tip flow within these M5 contours.

At the higher-speed, take-off condition the tip flows generated by the two rotors are much more similar. At this condition, a separate tip flow appears in the contours of each rotor as a concentrated region of highly turbulent flow off to the side of the blade wake. The four R4 data plots illustrate how the turbulent tip flow generated by this rotor changes with rotor speed. In contrast, since the tip flow generated by the M5 rotor only appears in the 100% speed contours, it is not clear how this tip flow changes with speed. Plans are in place to make additional measurements in the future with the M5 rotor operating at speeds between 60.8 and 100% speed, in order to track the changes of the M5 tip flow with rotor speed.

Figure 15 shows contours of average passage tangential turbulent velocity measured further downstream, at axial station LDV2. A comparison of these contours with those of figure 14 reveals that the turbulence generated by the rotors both diffuses (the turbulent regions get wider) and dissipates (the turbulent velocities decrease) as it moves downstream. The data presented in these figures indicates that although the turbulence is dissipating at all spanwise locations, it dissipates less rapidly in the tip region. Except for the case of the M5 rotor operating at 60.8% speed, all the plots presented for station LDV2 show the tangential turbulent velocities to be higher in the tip region than in the blade wake. The slower dissipation in the tip region may be due to the continuous production of turbulence in this region due to the high shear stress in the boundary layer along the outer endwall and/or to the radial migration of the blade wake unsteadiness into the tip region. In regards to broadband noise production, it appears that the tip flow unsteadiness becomes increasingly more important in relation to the blade wake unsteadiness as the wake flows move downstream. This is especially true at high rotor speeds where the tip flow unsteadiness is significantly higher than the blade wake unsteadiness.

Based on parts b) and e) of figure 15 which show results corresponding to the two rotors operating at approach, it is not clear which of these fan stages would be expected to generate less rotor/stator interaction broadband noise at this operating condition. As can be seen from these plots, the R4 blades generate higher peak levels of tangential turbulent velocity in the tip region; but they also generate significantly less turbulence inboard, primarily due to the much thinner blade wakes shed from the R4 blades. The acoustic results presented by Woodward et al (ref. 10) indicate that at approach the R4 stage generates higher broadband levels than the M5 at frequencies below 20 kHz, but lower broadband levels above this frequency. However, these noise levels correspond to the total broadband noise generated by the fan stages; that is, the contribution due to rotor wake/stator interaction has not been separated from the contributions of other sources. Therefore it is uncertain as to how much of these differences in the broadband noise levels result from the differences in the wake flows.

It is also unclear as to which rotor would generate less rotor/stator interaction broadband noise at the take-off operating condition. As can be seen from a comparison of parts d) and f) of figure 15, at take-off the R4 blades generate slightly more turbulence in the midspan region but less turbulence closer to the hub. The acoustic results (ref. 10) indicate that at this speed the R4 stage generated less broadband noise than the M5. However, once again, these acoustic results include the contributions of all the sources of broadband noise, not just the contribution resulting from rotor wake/stator interaction.

Shock Surveys: R4 Rotor

Data were acquired along the constant-radius survey locations denoted by the green line of figure 2b in an effort to determine the character of the shocks which exist on the R4 blades when operating at high rotor speeds. Figure 16 shows contours of average passage relative Mach number computed from the measured axial and tangential velocities. The left plot shows relative Mach number contours computed from measurements made at 87.5% speed (11,074 RPMC), while the right plot shows contours for 100% speed (12,657 RPMC). The upstream portion of the R4 blade cross-section at this radius (r=10.36" or 26.3 cm) is superimposed on the contours. The rotor blades would rotate downward in this view and the axial flow would be right-to-left. These contours clearly identify the normal shock which exists on the suction side of the rotor blades. This shock moves downstream along the suction side of the blade and increases in strength as rotor speed is increased from 87.5 to 100% speed. At 100% speed the shock has moved downstream to a location only about 10% of the rotor blade chord upstream of

the leading edge of the adjacent blade. Thus, the data are showing that even at 100% speed the shock does not move downstream far enough to be "swallowed" into the blade passage. With the shocks free to propagate upstream of the rotor it is likely that the strong perturbations of the mean flow created by the shocks are a significant source of tone noise emanating from the inlet.

Another view of the shock structure measured at 100% speed is depicted in figure 17. The left plot provided in the figure is a repeat of the 100% speed average passage relative Mach number contours presented in figure 16. The right plot also shows average passage relative Mach number contours measured at 100% speed, but here they are shown as computed from measurements made in the tip region during a constant-axial survey made at approximately 25% chord. The approximate axial location of the constant-axial survey (data shown in the right plot) is indicated by the dashed line in the left contour plot, while the radial location of the constant-radius survey (data shown in the right plot) is indicated by the dashed line in the right contour plot. The view depicted in the right plot is aft-looking-forward, so the rotor blades would rotate clockwise. The two black triangles overlayed on the contours represent regions where data could not be acquired because the blades blocked the field of view of the LDV receiving optics. The contours illustrate the extent of the supersonic and subsonic regions of the flow at this axial location and rotor speed. They also show the expected decrease in the shock strength with decreasing radius.

The blade-to-blade differences in the strength and position of the shocks are thought to be responsible for the generation of multiple pure tone noise (ref. 11). The plots of figure 18 illustrate the variation of the mean shock position across the blade passages. The contour lines plotted in the figures show an overlay of the Mach=1 contours measured in the 22 individual blade passages. Only contour lines corresponding to the deceleration of the flow through the shock are presented. The Mach=1 contours resulting from the acceleration of the flow to supersonic relative speeds in the expansion region between the shocks were omitted for clarity. These plots indicate that the variation of the shock position from passage-to-passage is roughly the same at the two speeds, spanning a distance equal to roughly 8% of the blade chord.

Tip Flow Surveys

Tip Flow Development: R4 Rotor

Data were acquired from constant-axial surveys in the tip region of the R4 rotor to obtain information on how the tip flows develop within the rotor blade passages. Previous investigations conducted at NASA Glenn indicate that the fan tip flow can migrate across the blade passage as it moves downstream (ref. 12 and 13). Figure 19 shows contours of tangential turbulent velocity measured near the outer case during the present study at seven axial locations within the model (the 5 tip flow and 2 wake survey locations). Contours are provided for two different rotor speeds; 61.7% speed data are plotted on the left and 87.5% speed data are plotted on the right. The contours for each speed are presented from top to bottom in the order of increasing downstream distance within the model. The data measured at the two different speeds show the same trend regarding the dissipation of the peak levels of turbulent velocity with downstream distance. That is, the peak levels are highest at the upstream-most axial station (25% chord); they then decrease while the tip flow thickens and moves downstream. Just downstream of the rotor, at 125% chord, the peak levels are roughly 2/3rds of the peak levels measured at 25% chord.

While the dissipation of the turbulence with axial distance in the tip region is similar at these two speeds, there are differences in the circumferential location of the tip flow within the passage. The tip flow measured at 61.7% speed is almost centered in the passage at 25% chord, and stays centered as it moves downstream. In contrast, at 87.5% speed and 25% chord, the tip flow is smaller in circumferential extent and is located much closer to the suction side of the blade. At 87.5% speed, as the tip flow moves downstream it appears to migrate away from the blade, toward the pressure side of the adjacent blade. By the time the flow reaches the downstream-most axial location, LDV2, the tip flow appears to have merged with the unsteadiness in the blade wake of the following blade.

Figure 20 shows the corresponding tangential turbulent velocities measured at the highest tested rotor speed, 100%. In this figure, the contours corresponding to the seven different axial locations within the model are presented twice; those presented at the left were all plotted using a single colorbar (that provided to the left of the contours), while the contour plots presented at the right were plotted using different colorbars (not shown), each having a range corresponding to the minimum and maximum turbulent velocities measured within each of the seven axial planes. Consequently, the left contours can be used to determine how the turbulent velocity levels vary with downstream distance, while the contours at the right provide a better view of the circumferential migration of the tip flow as it convects downstream. The line of turbulent flow extending radially inward from the outer case in the 25% chord contours is due to the normal shock located on the upstream portion of the blade shown previously in figure 16. This shock also shows up in the 50% chord contours as the region of unsteadiness just off the suction side of the blade. At this high speed condition, the tip flow extends only a short distance radially into the passage. The outermost part of the tip flow right next to the outer wall could not be measured due to increased optical noise levels associated with flare light off the window and blade tips. The data do, however, provide an indication of the location of the tip flow circumferentially within the blade passage. At 25% chord the tip flow is just off the suction side of the blade, between the blade and the shock. At 50% chord the tip flow is on the opposite side of the shock, roughly one-third of the blade gap off the suction side of the blade. As the flow moves downstream, the tip flow lags further and further behind the blade from which it was generated and, consequently, continues to migrate across the passage toward the pressure side of the following blade. At axial station LDV1 the tip flow appears to have migrated over to the wake of the adjacent blade. This migration of the tip flow to the adjacent blade wake did not occur until further downstream with the rotor at 87.5% speed. Thus, the data are indicating that the migration of the tip flow occurs more rapidly when the rotor speed is increased.

The tip flow data presented here indicate that the rotor wake plots need to be interpreted carefully. The close proximity of the blade wakes and tip flows in the downstream data plots might lead one to conclude that both emanated from the same blade. The data acquired within the passage indicates that this was not the case. Much of the highly unsteady flow near the fan case just to the pressure side of the blade wake shown in the downstream-most plots actually comes from the adjacent (preceding) blade.

The data also indicate that the entire chordwise extent of the blade tip does not contribute equally to the formation of the tip clearance flow, especially at high rotor speeds. In the 87.5 and 100% speed contours plotted in figures 19 and 20, the tip flow has already moved off the blade and into the passage at the 50% chord location. In addition, the data show

a decrease in the maximum turbulent velocity measured in the tip region with increasing downstream distance. This suggests that even at the upstream-most location at which tip flow data were obtained, 25% chord, the tip flow may already be dissipating. This would imply that the blade tip upstream of the 25% chord location is responsible for the generation of the tip clearance flow. This should not be too surprising considering that at these high rotor speeds a shock exists on the suction side of the blades (see fig. 16). It is likely that the blade loading is much higher upstream of the shock. This high loading would promote the development of the tip clearance flow.

Tip Clearance Effects: R4 Rotor

All of the R4 rotor data presented above were obtained with a rubstrip installed within the model which was designed to provide a 0.020" clearance between the blade tip and the fan case at the stacking axis of the rotor with the fan operating at 100% of its design speed. A limited amount of LDV data were also obtained with the R4 rotor with what was called a "nominal" rubstrip installed in the fan case. This nominal rubstrip was designed so that the fan would actually rub into the rubstrip at 100% speed, thus providing no clearance between the fan and the duct at this speed. With this nominal rubstrip installed, two LDV surveys were made in the tip region downstream of the R4 fan at axial station LDV1; one with the rotor operating at 87.5% speed, the other with the rotor at 100% speed. This data was obtained so that it could be compared to similar data obtained with the 0.020" clearance rubstrip installed. Such a comparison would illustrate how the tip flow changes with tip clearance.

Figure 21 shows contour plots which were made to illustrate the differences in the mean flows generated with the two different rubstrips installed. These contours depict the same parameter used earlier to illustrate the nonuniformities in the mean wake flows. That is, they depict the difference between the average passage mean tangential velocities and the circumferentially-averaged tangential mean velocity measured at a given location in the flow. This parameter is plotted because it is thought to be at least partially responsible for the generation of rotor/stator interaction tone noise. In the figure, plots are presented for both of the tested speeds, with 87.5% speed data plotted at the left and 100% speed data at the right. The contours plotted for both speeds indicate that the tip flow becomes stronger as the tip clearance is increased. This results in a more nonuniform mean flow.

The same result is indicated by the line plots of figure 22, which depict radial distributions of the perturbation in the mean tangential flows measured with the two rubstrips installed. As before, the term "perturbation" is used to represent the magnitude of the oscillation (max minus min) of the mean tangential flow at a given radial location. In figure 22, two plots are provided: the left plot shows the perturbations measured during runs made with each of the two rubstrips installed and with the R4 rotor operating at 87.5% speed; the right plot shows the corresponding results for the rotor operating at 100% speed. As can be seen, at both of the tested speeds the mean tangential flow perturbations are stronger with the larger tip clearance. One might expect the stronger mean flow perturbations associated with the larger tip clearance to generate higher levels of rotor/stator interaction tone noise.

The change in the total tone noise generated by the model resulting from the change in the rubstrips was measured during the acoustic testing. Figure 23 shows the measured increase in the 1BPF tone power level that resulted from changing from the nominal clearance rubstrip to the 0.020" clearance rubstrip. In this figure, the change in the 1BPF tone

power level is shown as a function of rotor speed. The data points corresponding to the operating conditions at which the LDV data were obtained (87.5 and 100% speed) are marked on the plot. At these two speeds there was almost no difference in the 1BPF tone power levels generated with the two different rubstrips installed. This seems to be indicating that the differences in the mean flows measured at this upstream axial station, LDV1, either 1) are not significant enough to generate measurable differences in the 1BPF tone levels, or, 2) if they are, that these differences diminish as the wake flows move downstream to the point that the two flows become essentially identical (from an acoustics standpoint) by the time they interact with the downstream stator vanes. Another possibility is that the measured tone levels are not controlled by the rotor/stator interaction noise. The acoustic results plotted in figure 23 are based on the total noise generated by the model, not just that due to rotor/stator interaction. The contribution resulting from rotor/stator interaction could not be separated from the total tone noise since acoustic data were not acquired with the barrier wall in place next to the model during the tip clearance studies. If the measured tone levels are controlled by another, more dominant source (such as inlet boundary layer/fan interaction, shock noise, or rotor self-noise), then any reductions in rotor-stator interaction tone noise could be masked by this other source.

The contour plots presented in figure 24 are provided to illustrate how the unsteadiness in the tip region downstream of the rotor varies with tip clearance. This figure shows a comparison of average passage tangential turbulent velocities measured with the two different rubstrips installed. Once again, plots are provided for both of the tested rotor speeds, with 87.5% speed data plotted at the left, and 100% speed data at the right. The tip flow disturbance generated with the larger tip clearance is shown to extend radially approximately 30% further into the passage. Also, the peak levels of tangential turbulent velocity are higher with the larger tip gap — about 15% higher at 87.5% speed and 25% higher at 100% speed. In agreement with the above mean flow results, these turbulence data are indicating that the tip flow gets stronger and more pronounced as the tip clearance gap is increased.

Conclusions

1) Contour plots were provided which illustrate the differences in the mean wake flows generated by the R4 and M5 rotors at their respective approach operating conditions. These data show that:
a) The M5 blade wakes were thicker than R4 blade wakes.
b) The M5 blade wakes were leaned in a direction opposite to the direction of rotor rotation.
c) At the upstream wake axial location, LDV1, the lean of the M5 wakes was about the same at all radial locations (the wakes were leaned, but straight). At the downstream axial location, LDV2, the lean of the M5 blade wakes increased with increasing radius (the wakes were curved).
d) The M5 wakes became more skewed (exhibited more lean) as they moved downstream.
e) Over approximately the inner 75% of the blade span the lean of the R4 wakes was similar to that of the M5 wakes. However, in the tip region the R4 wakes had very little lean. The differences in the wake shapes were used to provide a possible explanation for the lower rotor stator interaction tone noise produced by the M5 rotor at the approach condition.

2) Contour plots were provided which illustrate the differences in the mean wake flows generated by the R4 and M5 rotors at their respective take-off operating conditions. At the downstream axial location, LDV2, the mean wake flow of the M5 rotor was found to be more uniform than that of the

R4 rotor. As might be expected based on this result, the 2BPF and 3BPF rotor/stator interaction tone levels generated by the M5 stage were shown to be lower than those generated by the R4 stage at this speed. (There was little difference in the 1BPF tone power levels.)

3) Contour plots were also provided which depict the unsteadiness in the wake flows downstream of the two rotors. The tangential turbulent velocity contours that were provided indicate that for both rotors:
a) The turbulent regions in the wake flows became thinner with increasing rotor speed.
b) The turbulent velocities increased with increasing rotor speed.
c) The increase in turbulent velocity with rotor speed occurred more rapidly in the tip region than in the blade wake.
d) At a given operating condition the two rotors generated comparable peak levels of tangential turbulent velocity.

4) These turbulent wake flow plots also indicate that at their respective approach operating conditions there was a significant difference in the character of the unsteadiness produced by the two rotors. At approach:
a) A thick region of unsteady flow extended completely across the R4 rotor blade passages.
b) The flow downstream of the tips of the M5 blades was much less turbulent.
c) The R4 blades generated higher peak levels of tangential turbulent velocity than the M5 blades in the tip region, but less turbulence inboard.

5) At take-off, the unsteady wake flows of the two rotors were more similar. Both wake flows contained a concentrated region of highly turbulent flow due to the presence of a tip vortex.

6) The dissipation and diffusion of the wake flow turbulence of both rotors was illustrated by plots showing the flows at two axial stations downstream of the rotor. These plots indicate that the unsteadiness in the blade wakes dissipates more rapidly than the unsteadiness in the tip region.

7) Contour plots of relative Mach number were provided which illustrate the mean location of the shocks emanating from the R4 blades at both 87.5 and 100% speed. These data show:
a) The shock moves downstream as the rotor speed is increased from 87.5 to 100% speed.
b) At both 87.5 and 100% speed, the shock extends upstream of the leading edge of the following blade (ie. the shock is not swallowed).
c) The variation of the mean shock position from passage-to-passage is roughly the same at the two speeds, spanning a distance equal to roughly 8% of the blade chord.

8) Contour plots were presented which illustrate the propagation of the tip flow both within and downstream of the blade passage. These show that:
a) At 61.7% speed a relatively thick region of unsteady flow extends across the blade passage in the tip region. The point of maximum unsteadiness within this region stays roughly centered between the two adjacent blades (and blade wakes) as it moves downstream.
b) As the rotor speed is increased the tip flow becomes smaller and more localized.
c) At high speed (87.5 and 100%) the tip flow migrates from the suction surface of the blade from which it was formed toward the adjacent (following) blade. This migration of

the tip flow occurs more rapidly as rotor speed is increased. Downstream of the rotor the tip flow merges with the blade wake of the adjacent (following) blade.
d) The upstream portion of the blade tip is responsible for generating the tip flow.

9) Contour plots were presented which illustrate the effect of changes of the R4 rotor blade tip clearance on the flow downstream of the tip. LDV data were obtained with two different rubstrips installed in the model; one designed to provide a clearance of 0.020" between the blade tips and the case with the R4 fan at 100% speed, the other designed so that the fan would rub into the case with the fan at 100% speed. LDV data obtained at 87.5 and 100% speed showed that the nonuniformities in the mean wake flow increased with increasing tip clearance. These increases were not accompanied by increases in the 1BPF tone power levels generated by the model. This may be indicating that the mean flow differences dissipated by the time the flows interacted with the stators, or that the tone noise was controlled by some source other than rotor blade tip wake/stator vane interaction.

References

1. Envia, E., "Fan Noise Reduction: An Overview," AIAA Paper 2001-0661, 2001.

2. Martens, S., Shin, H., and Gliebe, P.,"Rotor Wake Unsteady Flowfield Hot-wire Measurements in the Universal Propulsion Simulator (UPS) at NASA," GE Aircraft Engines TM 9767.

3. Ganz, U.W.,, "Experimental Investigation of the Unsteady Flow Characteristics in the Boeing 18-Inch Fan Rig," AIAA Paper 99-1886, 1999.

4. Podboy, G.G., "Further Analysis of Fan Wake Data Obtained Downstream of the Allison Low Noise Fan and the Pratt & Whitney ADP Fan 1" Models," AST Engine Noise Workshop, Vol IV, pp. 131-160, April 1998.

5. Podboy, G.G., Krupar, M.J., Helland, S.M., and Hughes, C.E., "Steady and Unsteady Flow Field Measurements Within a NASA 22-Inch Fan Model," AIAA Paper 2002-1033, 2002.

6. Verhoff, V.G., "Three-Dimensional Laser Window Formation," NASA/RP 1280, 1992.

7. Brookfield, J.M., Waitz, I.A., and Sell, J., "Wake Decay Effect of Freestream Swirl," *Journal of Propulsion and Power*, Vol. 14, No. 2, pp 215-224, Mar.-Apr. 1998.

8. Envia, E., and Nallasamy, M., "Design Selection and Analysis of a Swept and Leaned Stator Concept," *Journal of Sound and Vibration,* Vol. 228, No. 4, December 1999.

9. Envia, E. "Influence of Vane Sweep on Rotor-Stator Interaction Noise," Ph.D. Dissertation, University of Arizona, 1988.

10. Woodward, R.P., Hughes, C.E., Jeracki, R.J., and Miller, C.J., "Fan Noise Source Diagnostic Test —Far-field Acoustic Results," AIAA Paper 2002-2427, 2002.

11. Hayden, R.E., Bliss, D.B., Murray, B.S., Chandiramani, K.L., Smullin, J.I., Schwaar, P.G., "Analysis and Design of a High Speed, Low Noise Aircraft Fan Incorporating Swept Leading Edge Rotor and Stator Blades," NASA CR-135092, 1977.

12. Suder, K.L., and Celestina, M.L., "Experimental and Computational Investigation of the Tip Clearance Flow in a Transonic Axial Compressor Rotor," *Journal of Turbomachinery*, Vol. 118, pp. 218-229, 1996.

13. Van Zante, D.E., Strazisar, A.J., Wood, J.R., Hathaway, M.D., Okiishi, T.H., "Recommendations for Achieving Accurate Numerical Simulation of Tip Clearance Flows in Transonic Compressor Rotors," ASME Paper 99-GT-390, 1999.

Figure 1. Source Diagnostic Test model installed in the
NASA Glenn 9 X 15 Foot Wind Tunnel

a) Survey Locations Relative to M5 Fan Stage

b) Survey Locations Relative to R4 Fan Stage
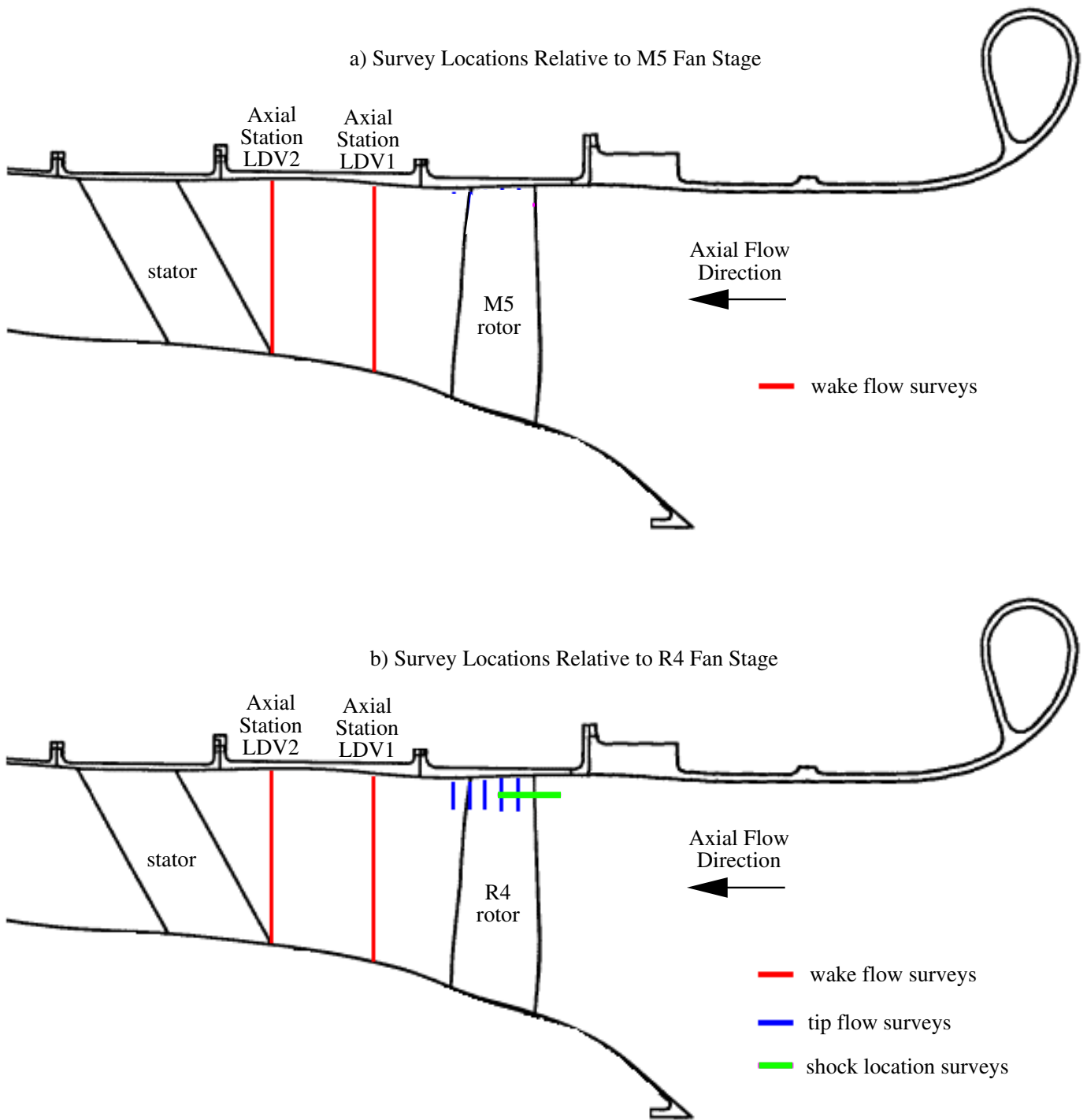
Figure 2. Schematic showing side view of model and location of LDV
surveys made using the M5 (top) and R4 (bottom) rotors.

Figure 3. LDV system hardware installed next to the SDT model in the
NASA Glenn 9 X 15 Foot Wind Tunnel.
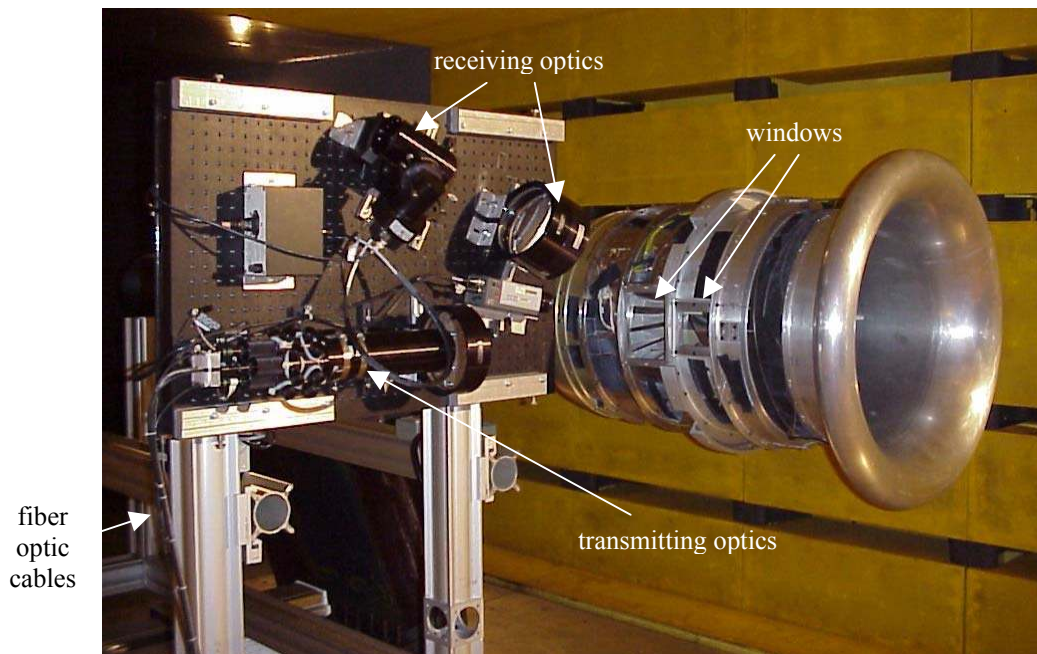
Figure 4. Photo of LDV optics mounted to traverse.

downstream
window

swept
stators

upstream
window

R4
rotor
blade
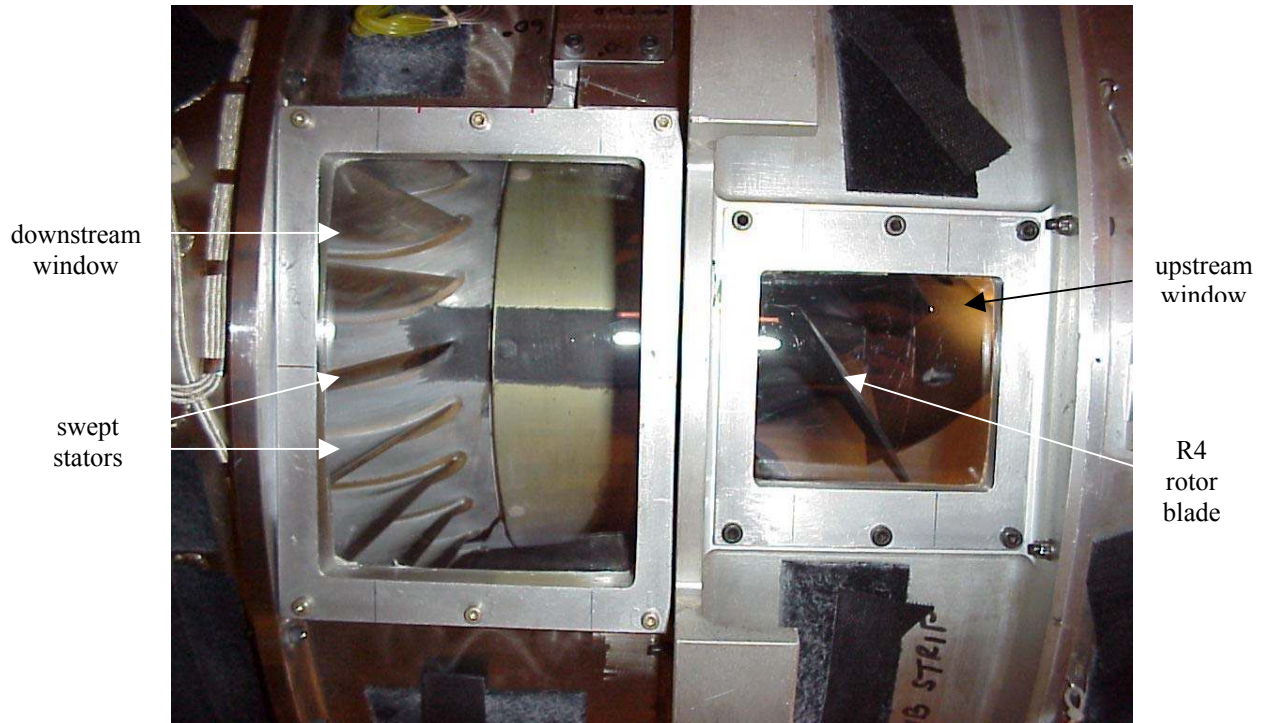
Figure 5. Photo of windows installed in the SDT model.

length of
white line
corresponds
to one micron
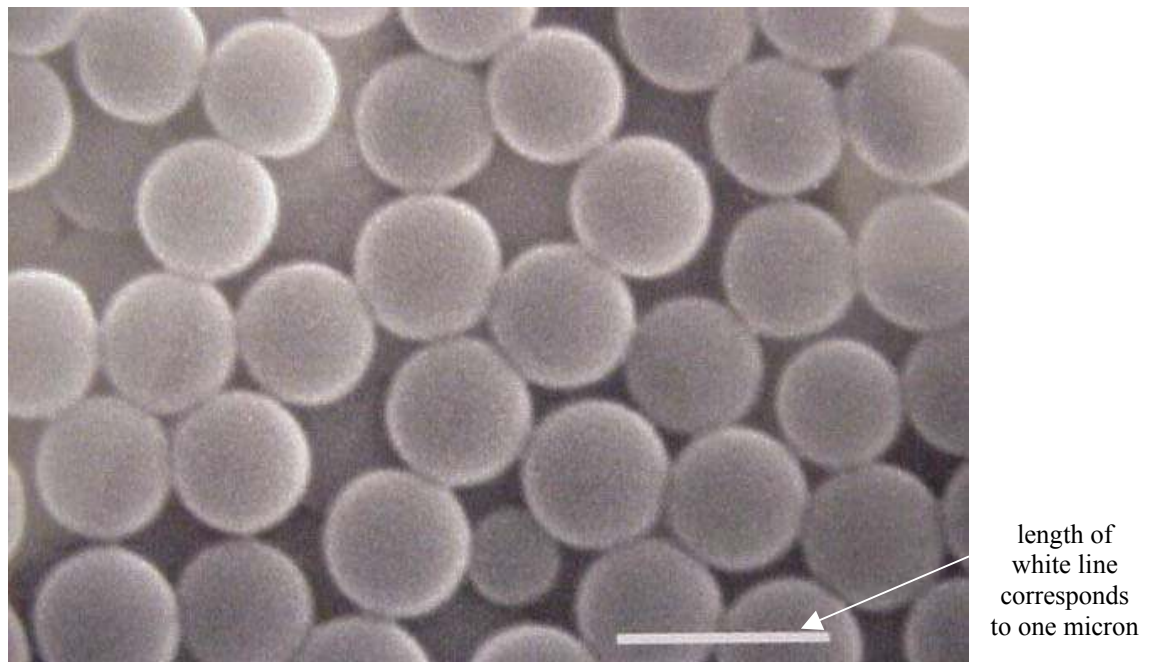
Figure 6. Scanning electron microscope photo of polystyrene latex
particles used as LDV seed.

a) Raw, unaveraged velocities sorted into 1100 circumferential bins.

b) Mean velocity profile across complete rev.

c) Turbulent velocity (rms of measurements) across complete rev.

folded   mean

folded   mean

d) "average passage"
mean velocities

e) "average passage"
turbulent velocities
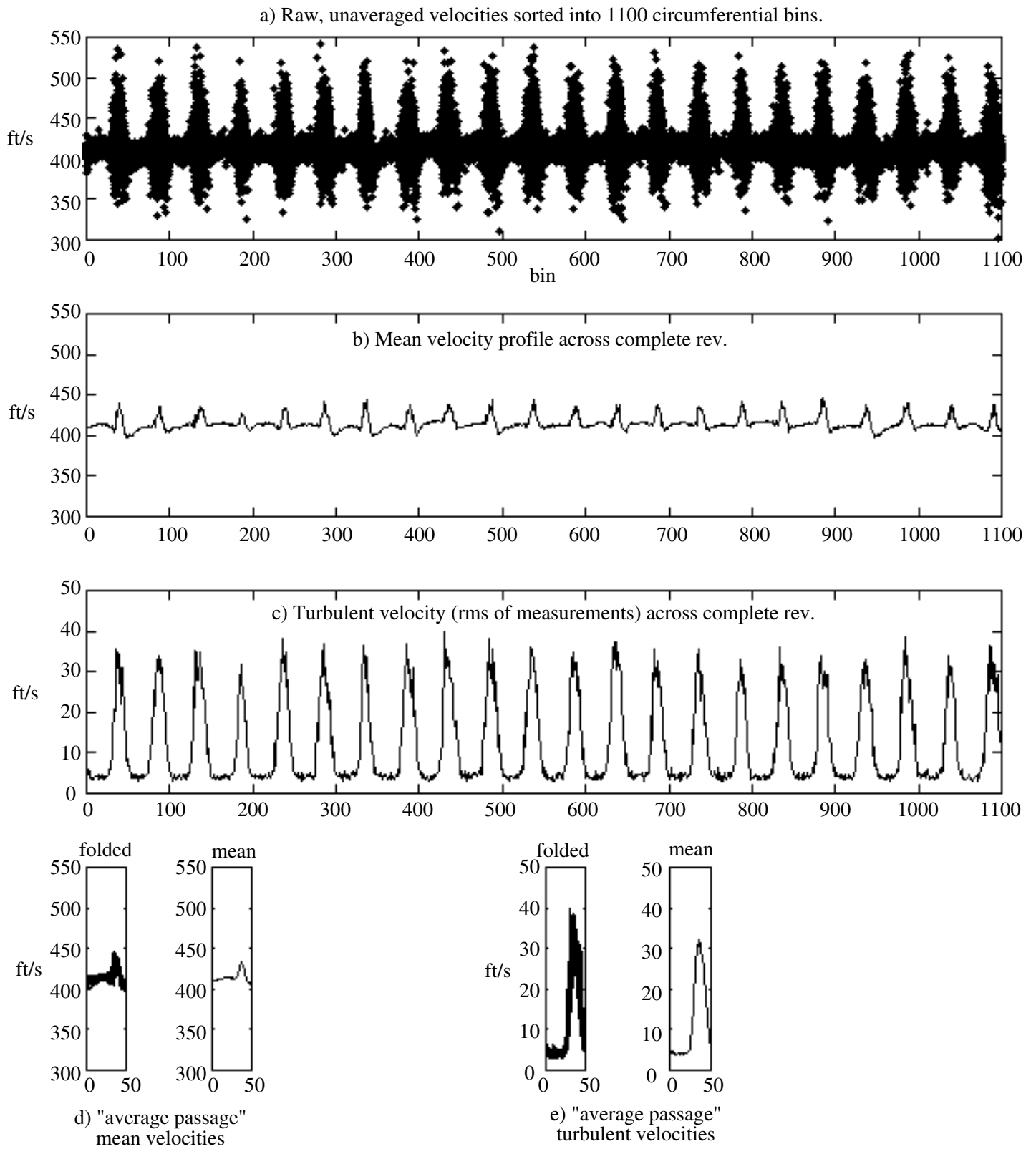
Figure 7. Illustration of LDV data reduction process.
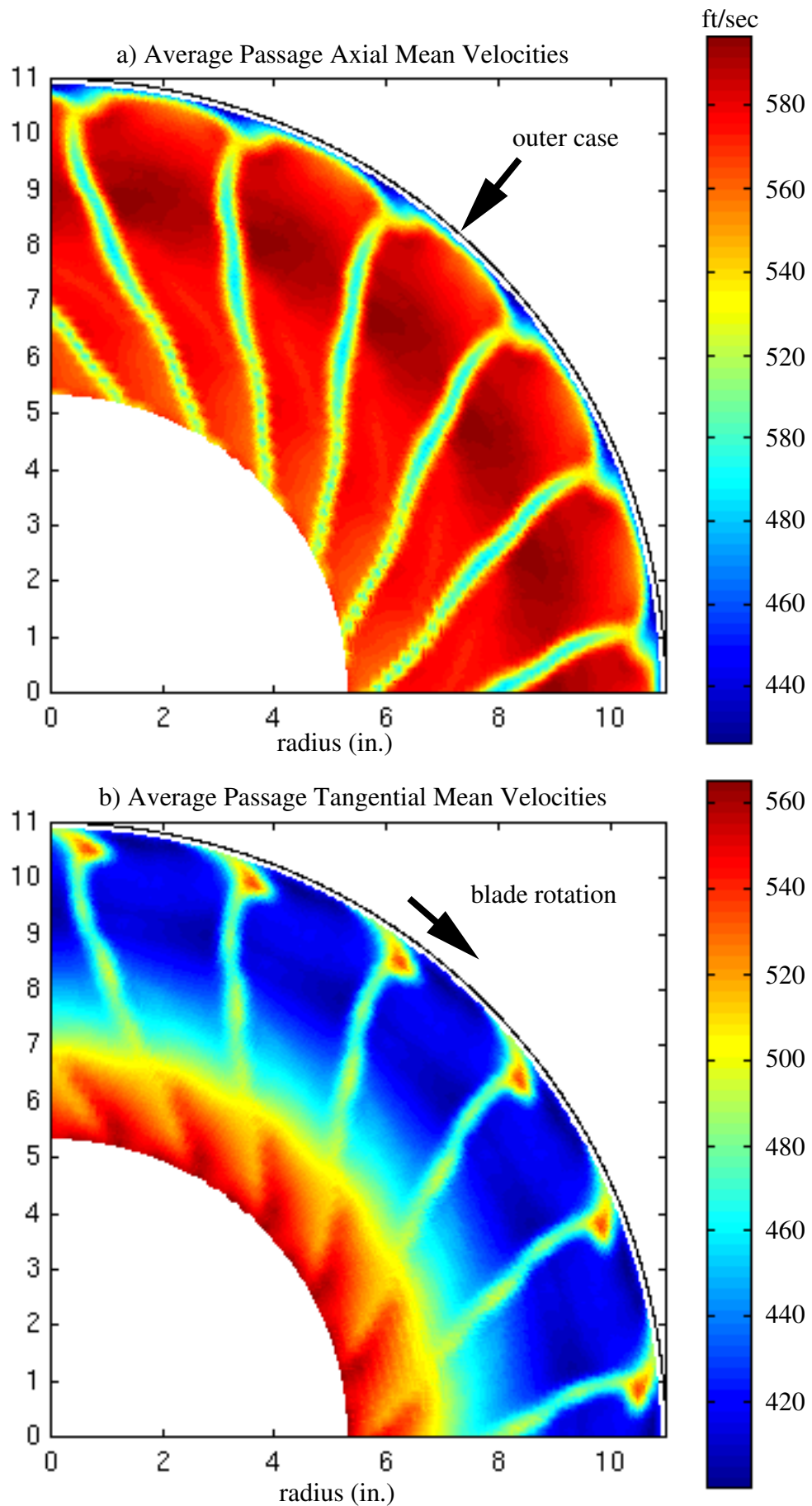
Figure 8. Average passage mean velocities measured downstream of the R4 rotor at axial station LDV1 with the rotor at 100% rotor speed.
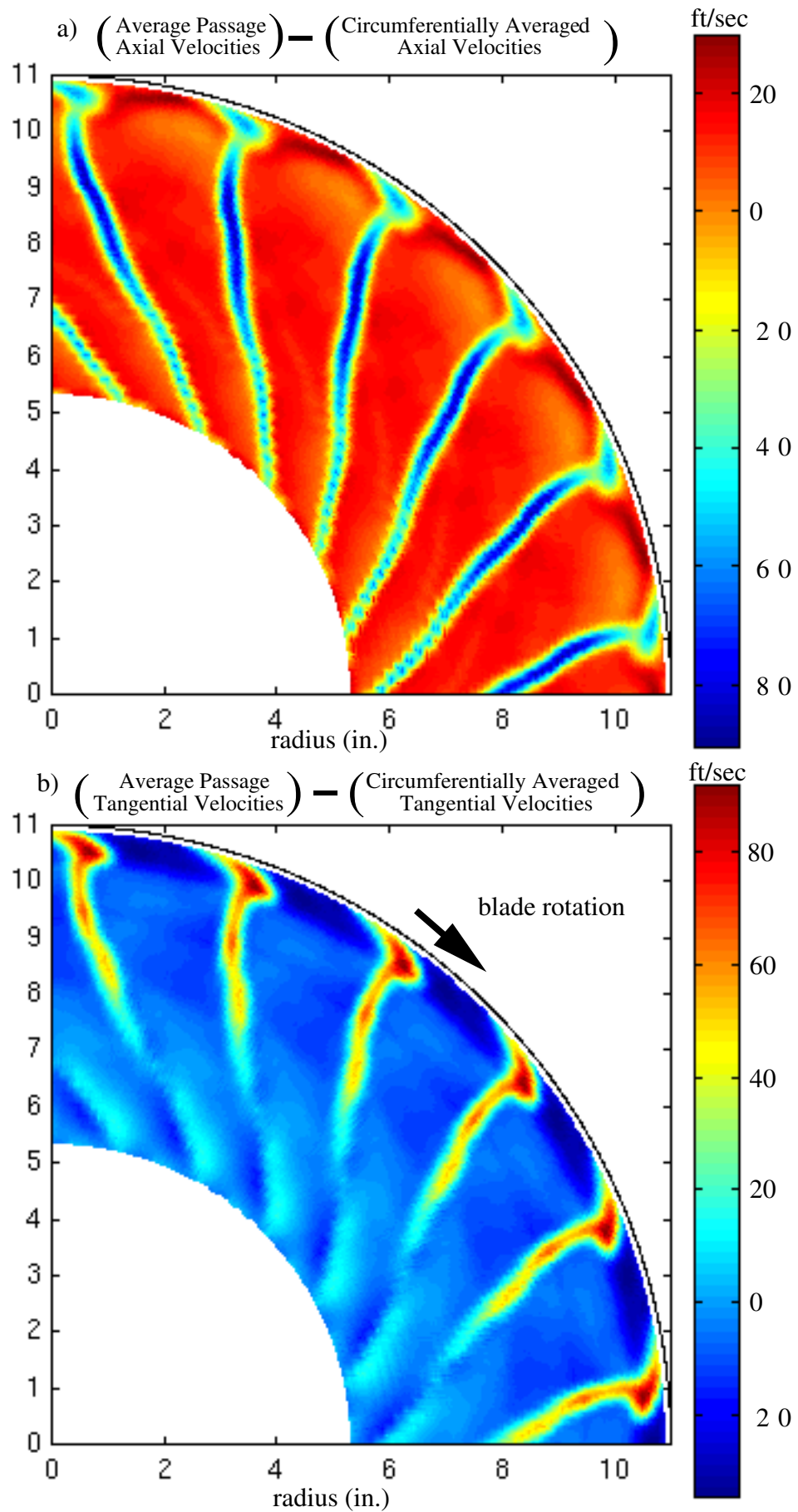
Figure 9. Difference between average passage mean velocities and circumferentially averaged velocities measured downstream of the R4 rotor at axial station LDV1 and 100% rotor speed.
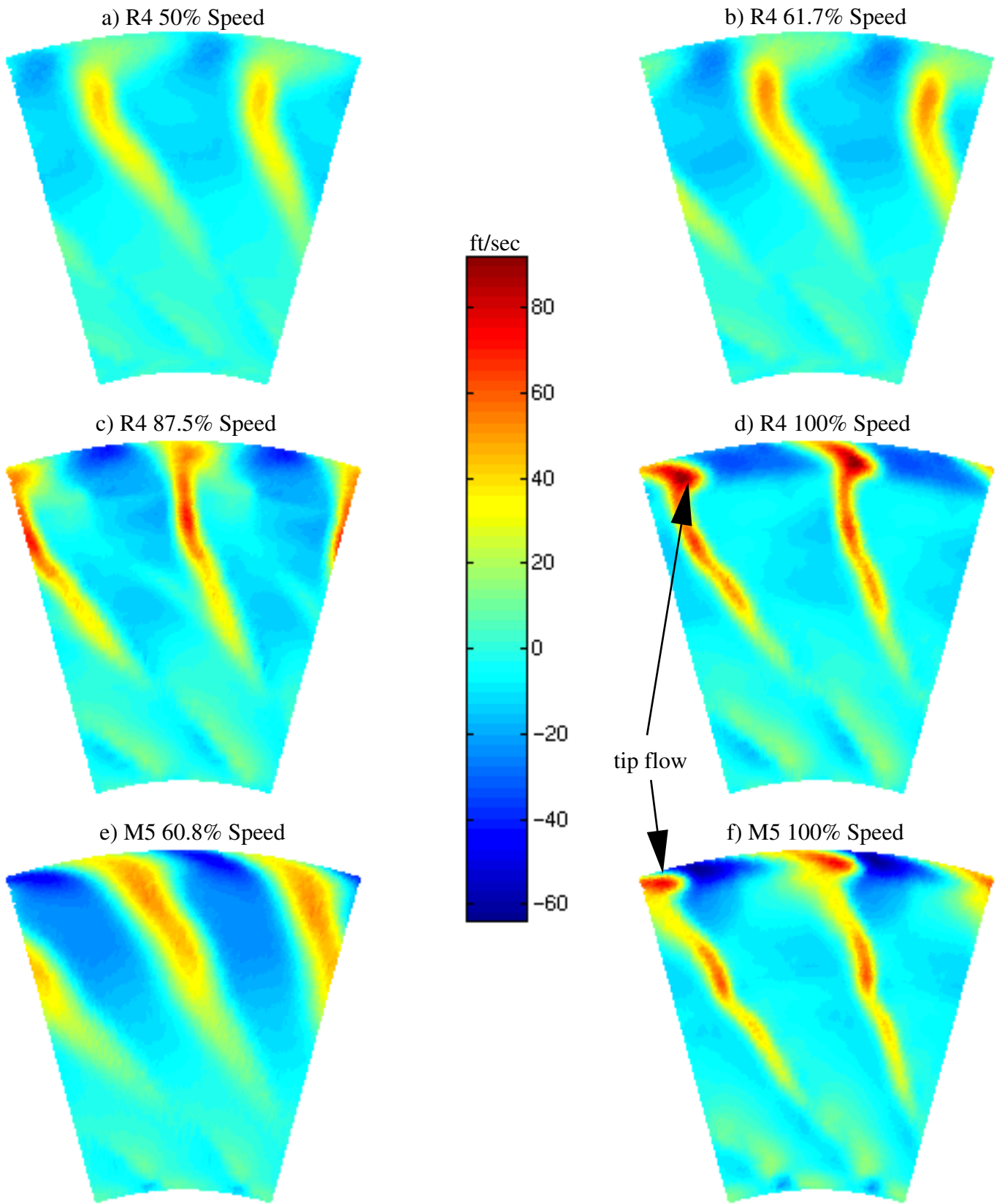
Figure 10. Difference between average passage tangential mean velocities and circumferentially averaged tangential velocities measured downstream of the R4 (parts a-d) and M5 (e-f) rotors at axial station LDV1.
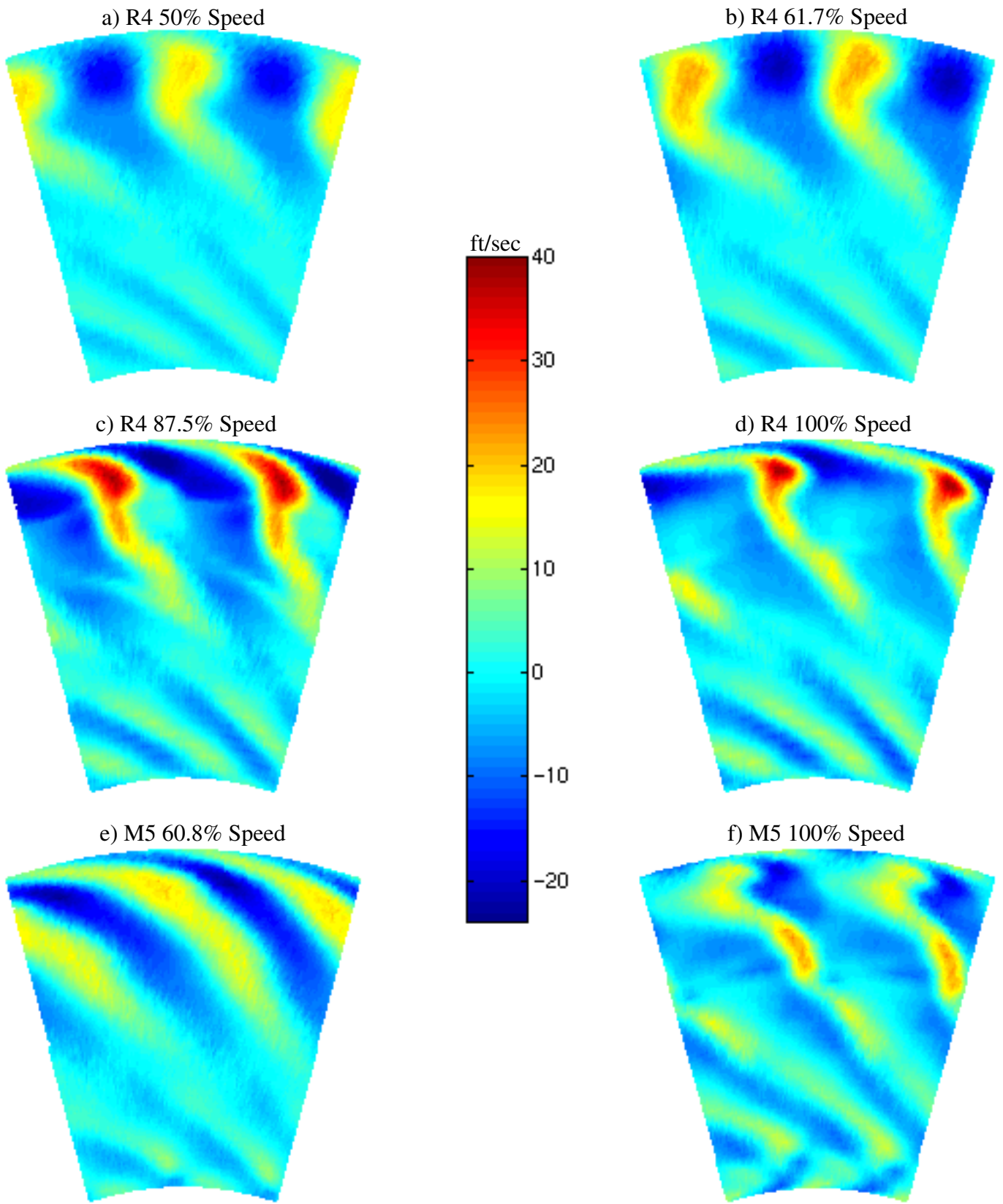
Figure 11. Difference between average passage tangential mean velocities and circumferentially averaged tangential velocities measured downstream of the R4 (parts a-d) and M5 (e-f) rotors at axial station LDV2.
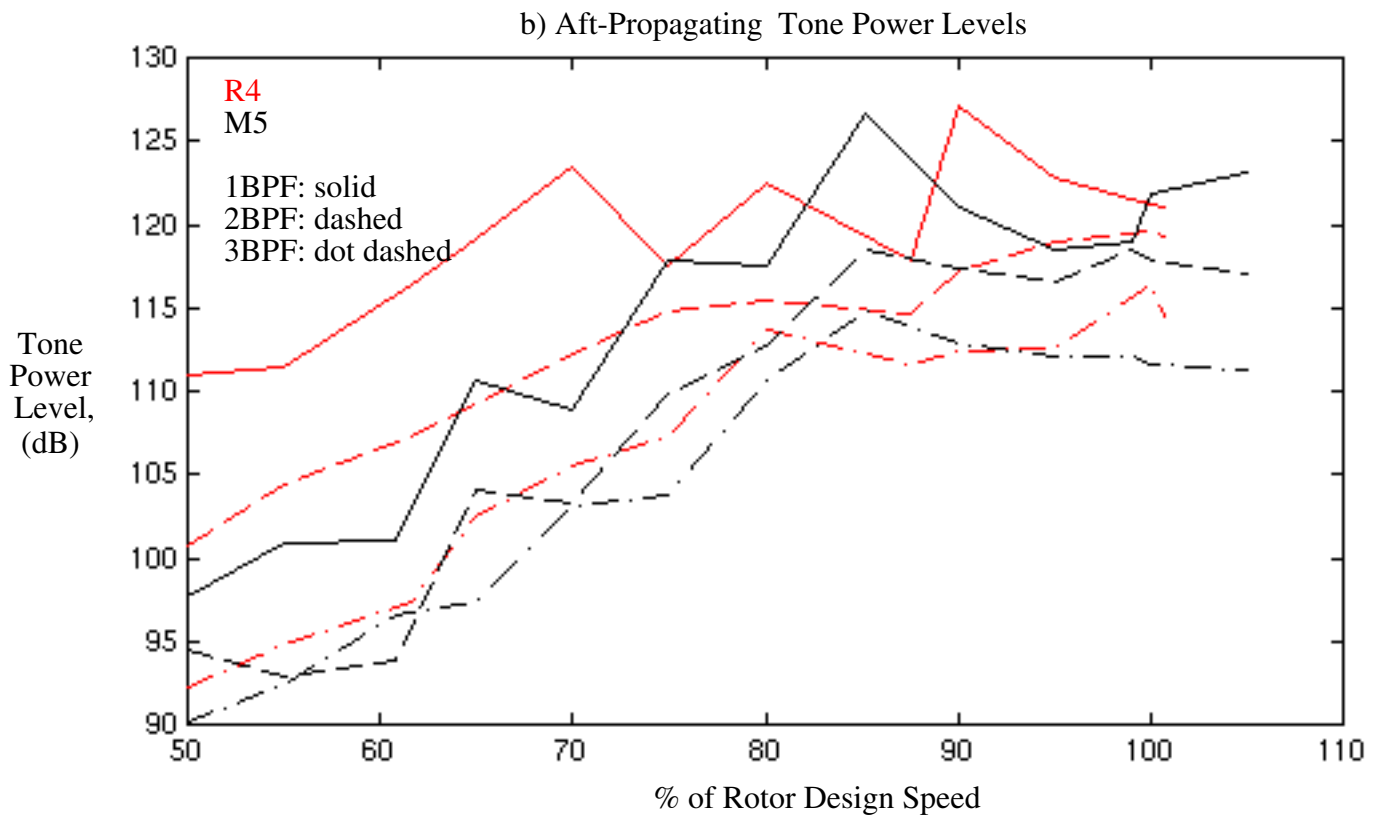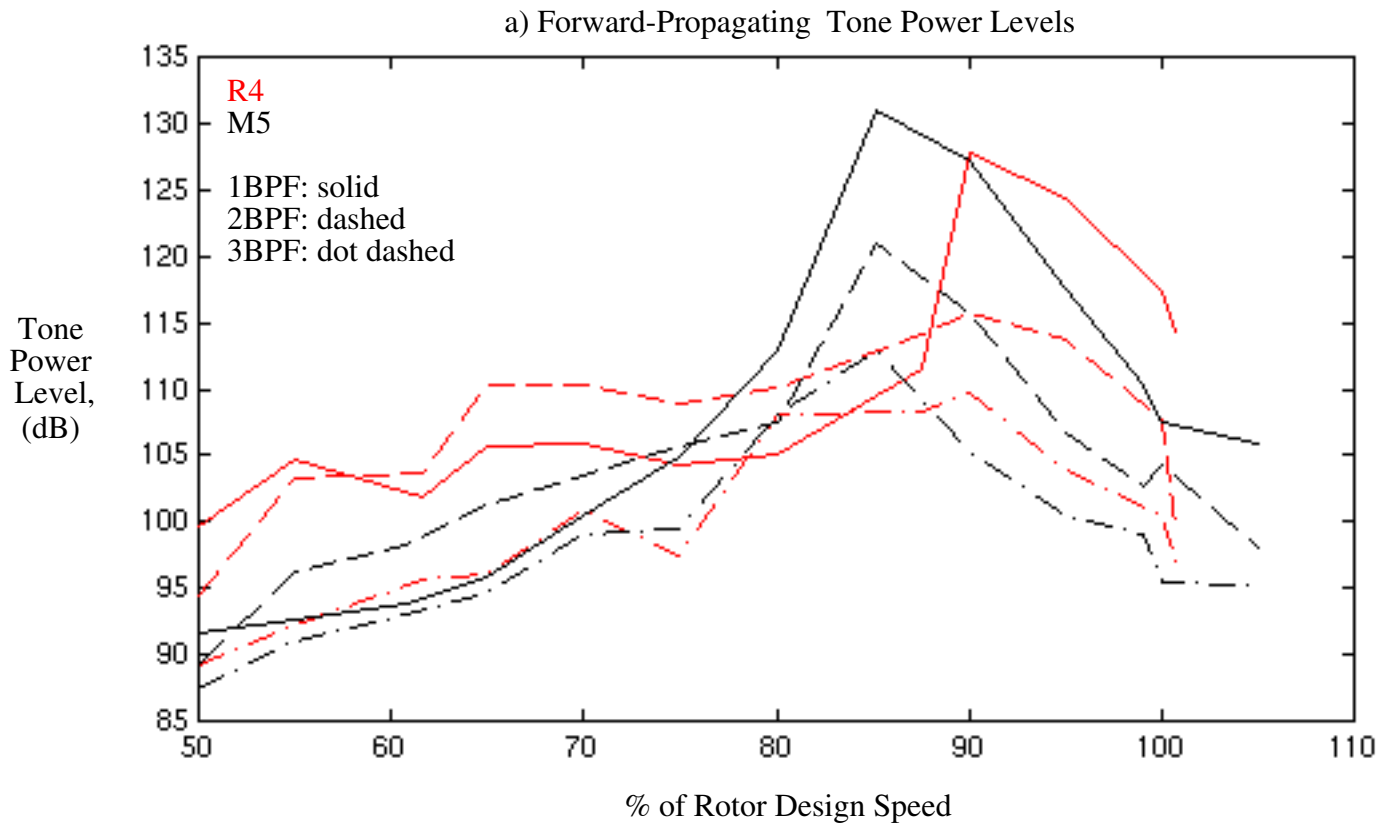
Figure 12. Tone power levels of forward (part a) and aft propagating (part b) noise measured for the R4 (shown in red) and M5 (black) fan stages over a range of operating speeds.
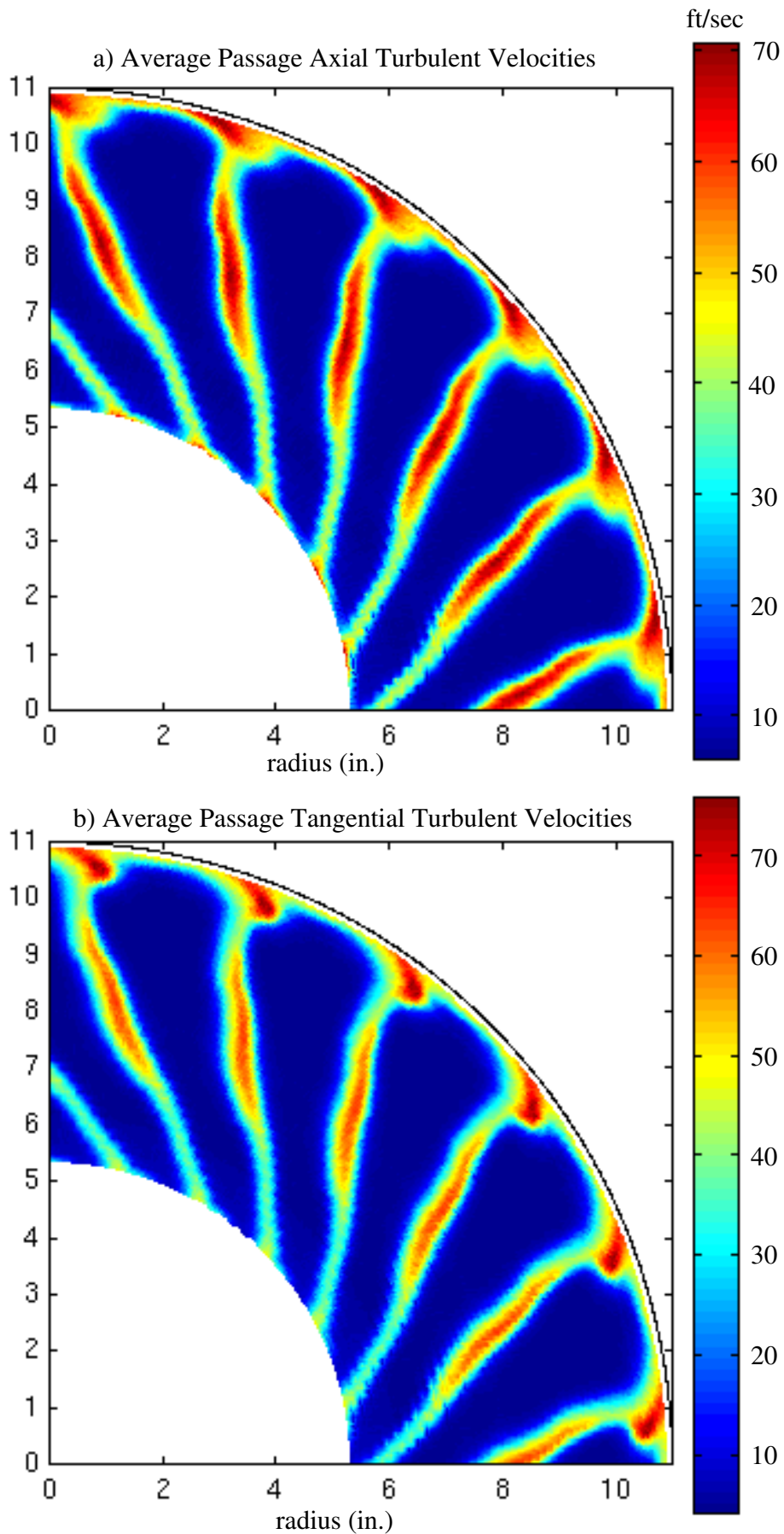
Figure 13. Average passage turbulent velocities measured downstream of the R4 rotor at axial station LDV1 at 100% rotor speed.
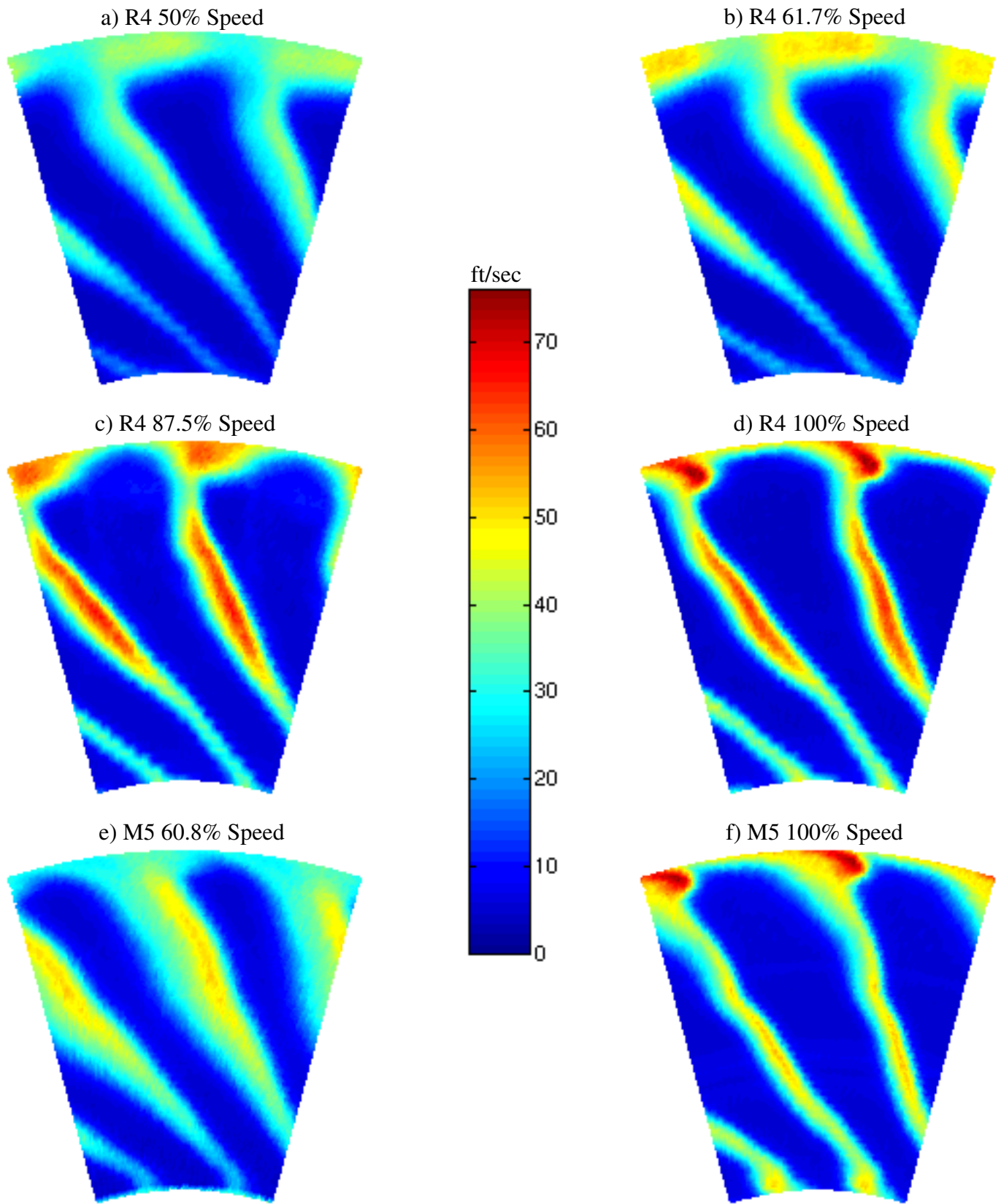
Figure 14. Average passage tangential turbulent velocities measured downstream of the R4 (parts a-d) and M5 (parts e-f) rotors at axial station LDV1.
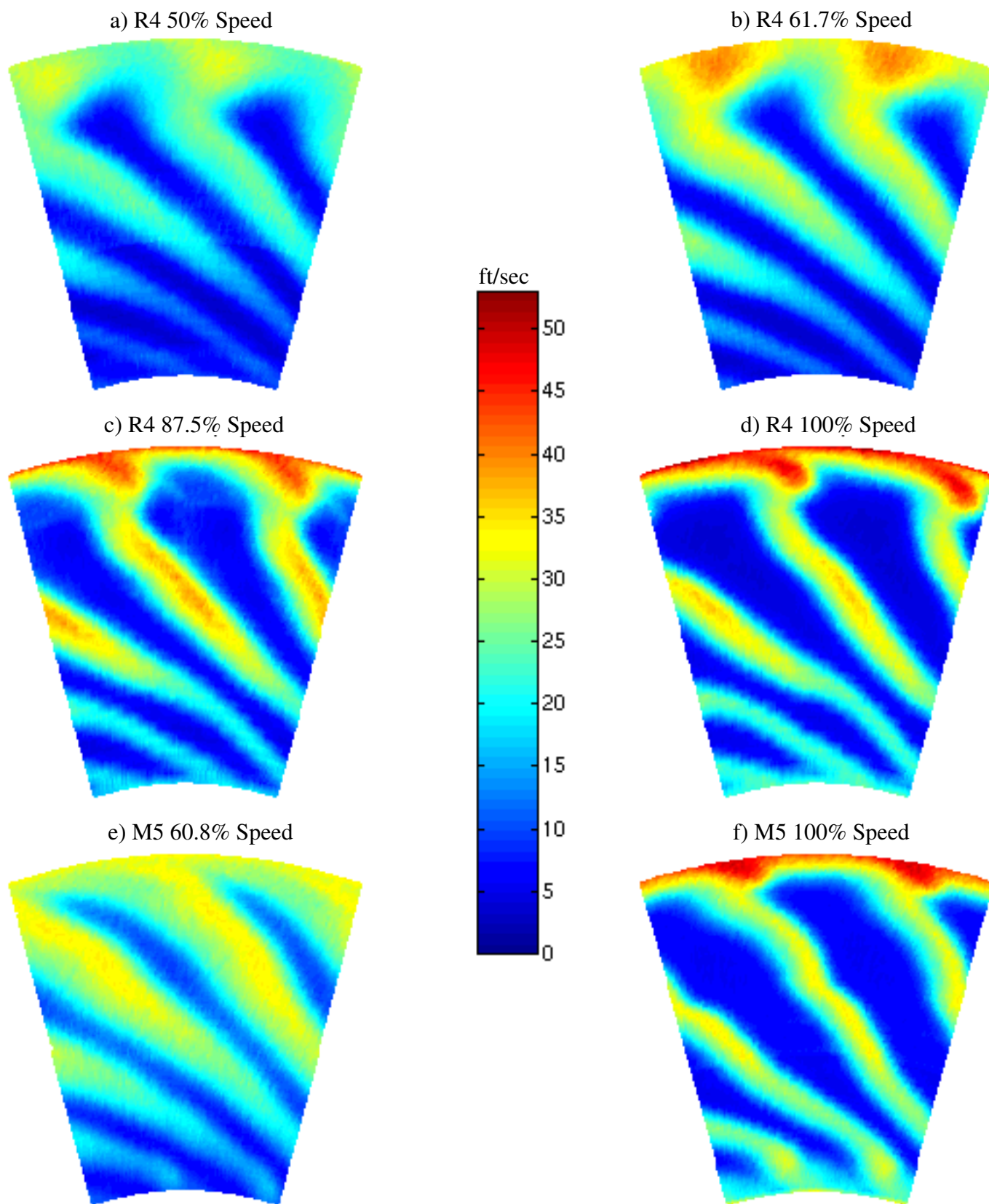
Figure 15. Average passage tangential turbulent velocities measured downstream of the R4 (parts a-d)
and M5 (parts e-f) rotors at axial station LDV2.
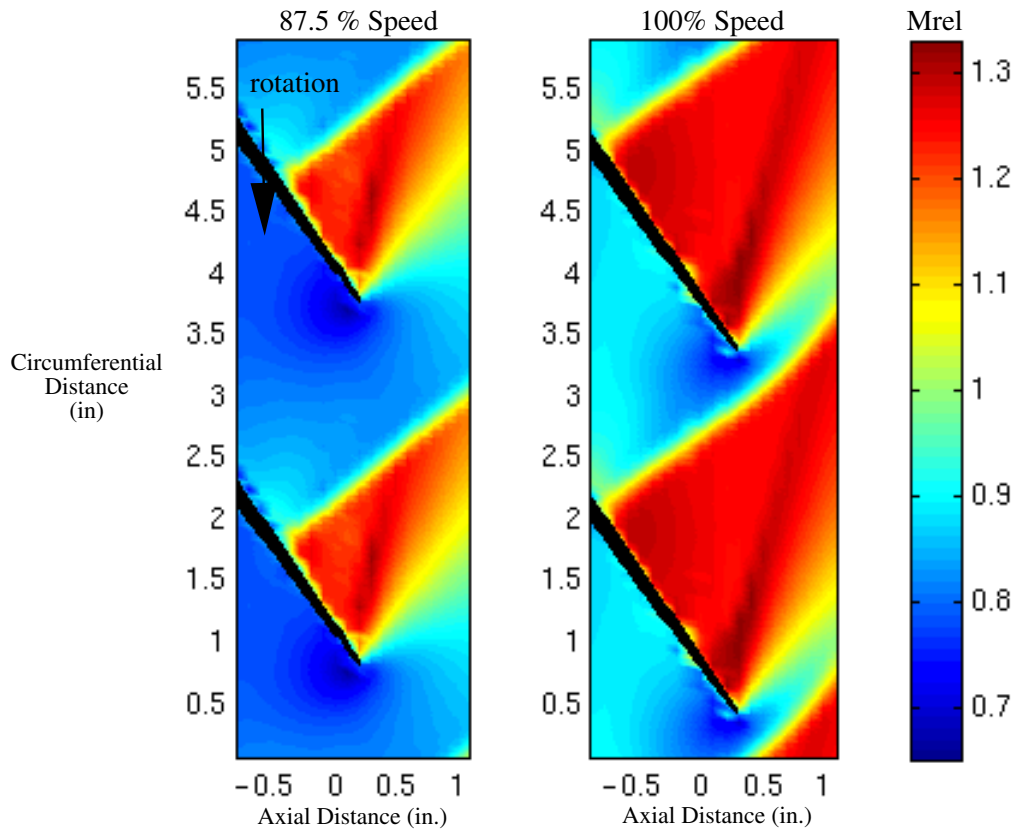
Figure 16. Average passage relative Mach number contours from constant-radius shock location surveys at r=10.36" (26.31 cm) within and upstream of the R4 blade passages.
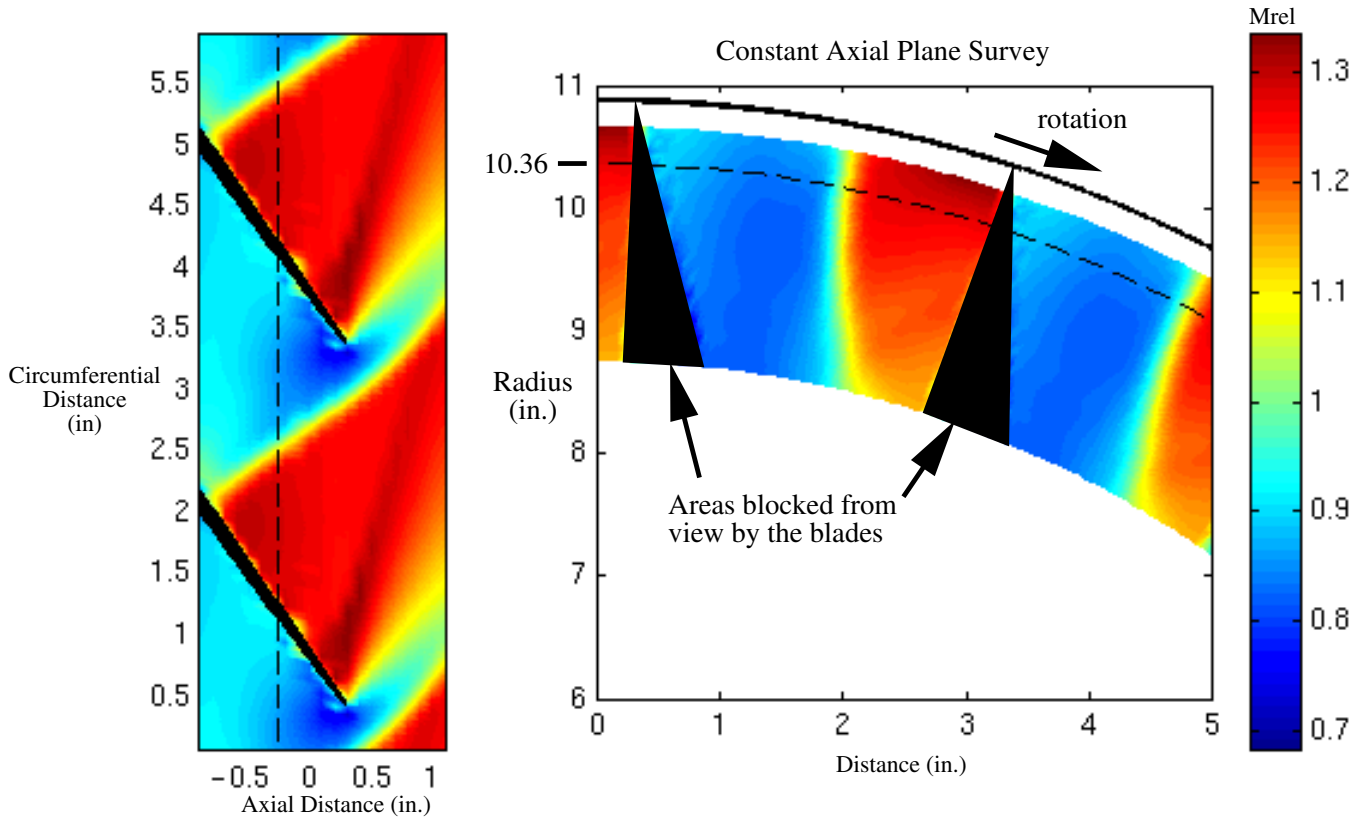
Figure 17. Average passage relative Mach number contours for the R4 rotor operating at 100% speed. Left plot is data acquired from constant-radius survey at r=10.36". Right plot is data acquired from constant axial survey made at approximately 25% chord.
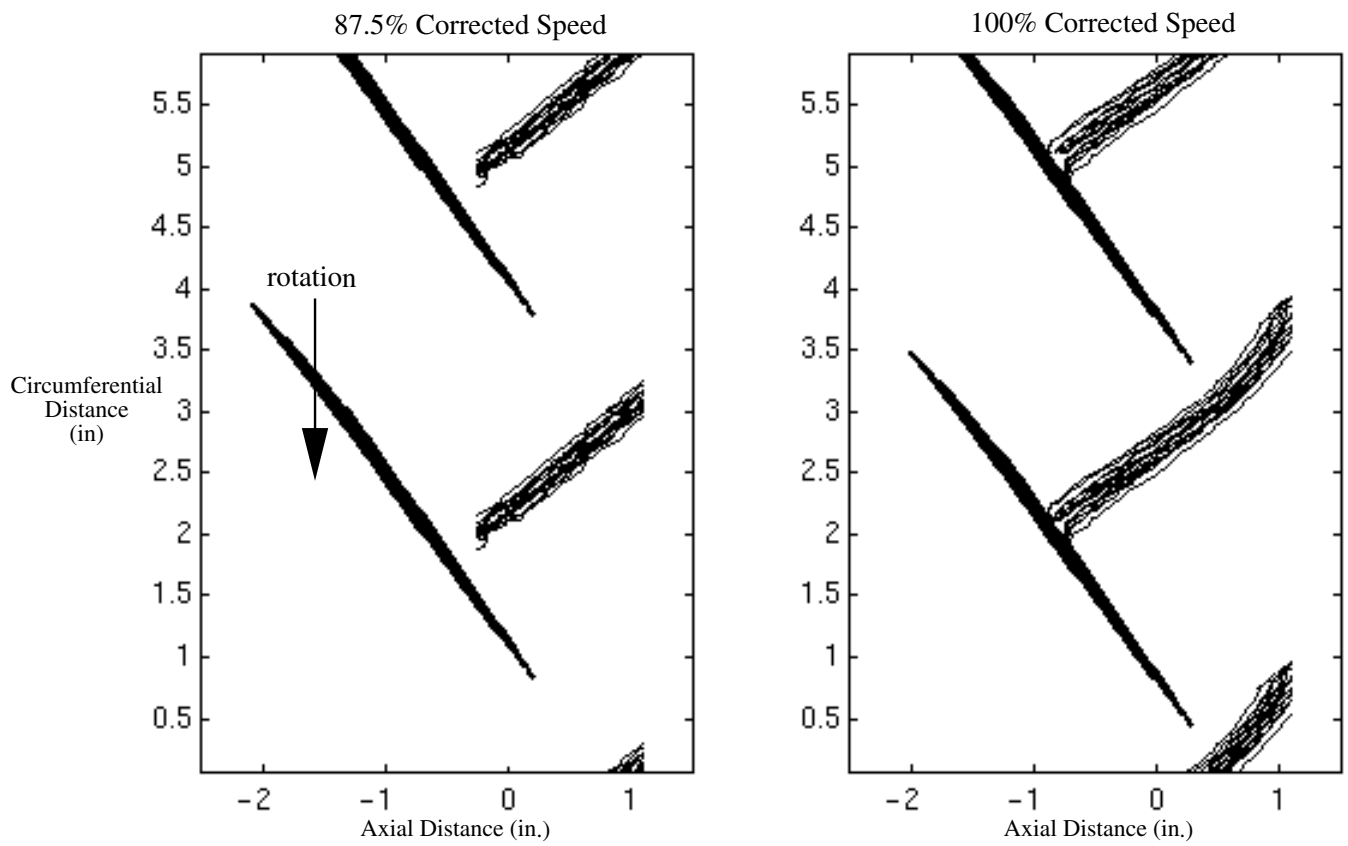
Figure 18. Overlay of Mach = 1.0 contours measured in the 22 blade passages of the R4 rotor at 87.5 (left plot) and 100% (right plot) corrected speed.
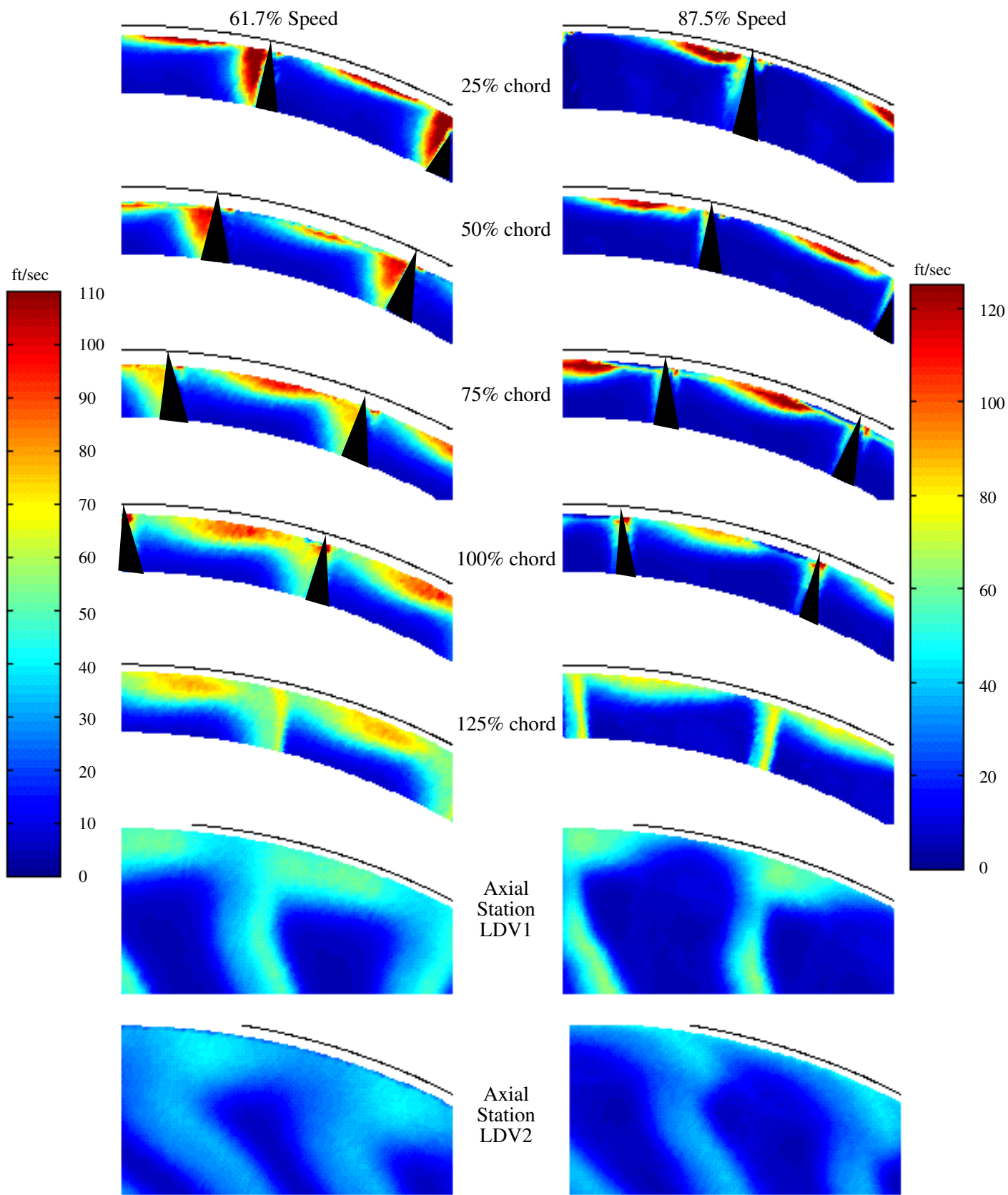
Figure 19. Contours of tangential turbulent velocity showing the tip flow within the blade passage and downstream of the R4 rotor at two speeds, 61.7% (left) and 87.5% (right
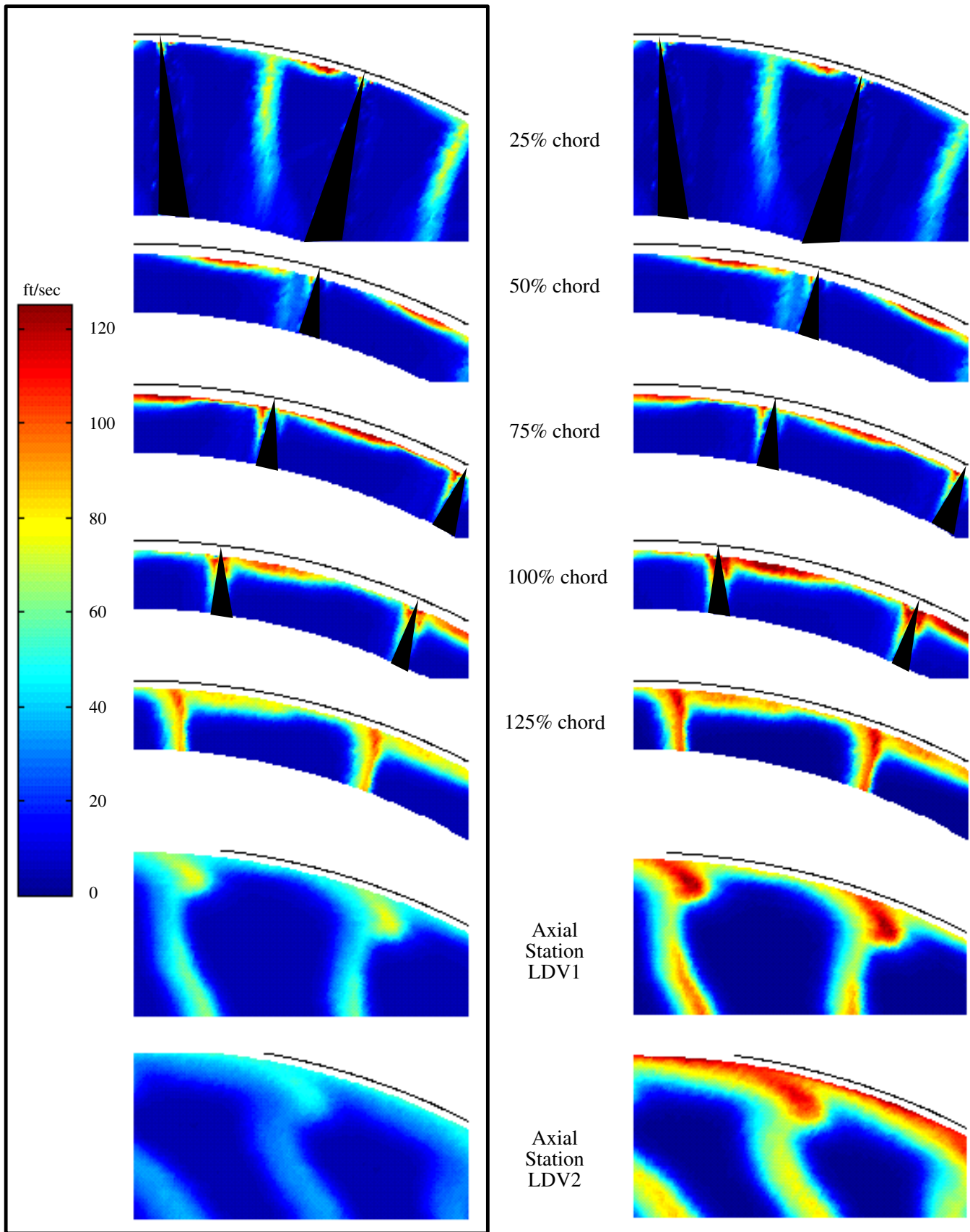
Figure 20. Contours of tangential turbulent velocity showing the tip flow within the blade passage and downstream of the R4 rotor at 100% speed. Plots within the box use the single colorbar shown at the left. Each plot at the right uses a different colorbar (not shown).
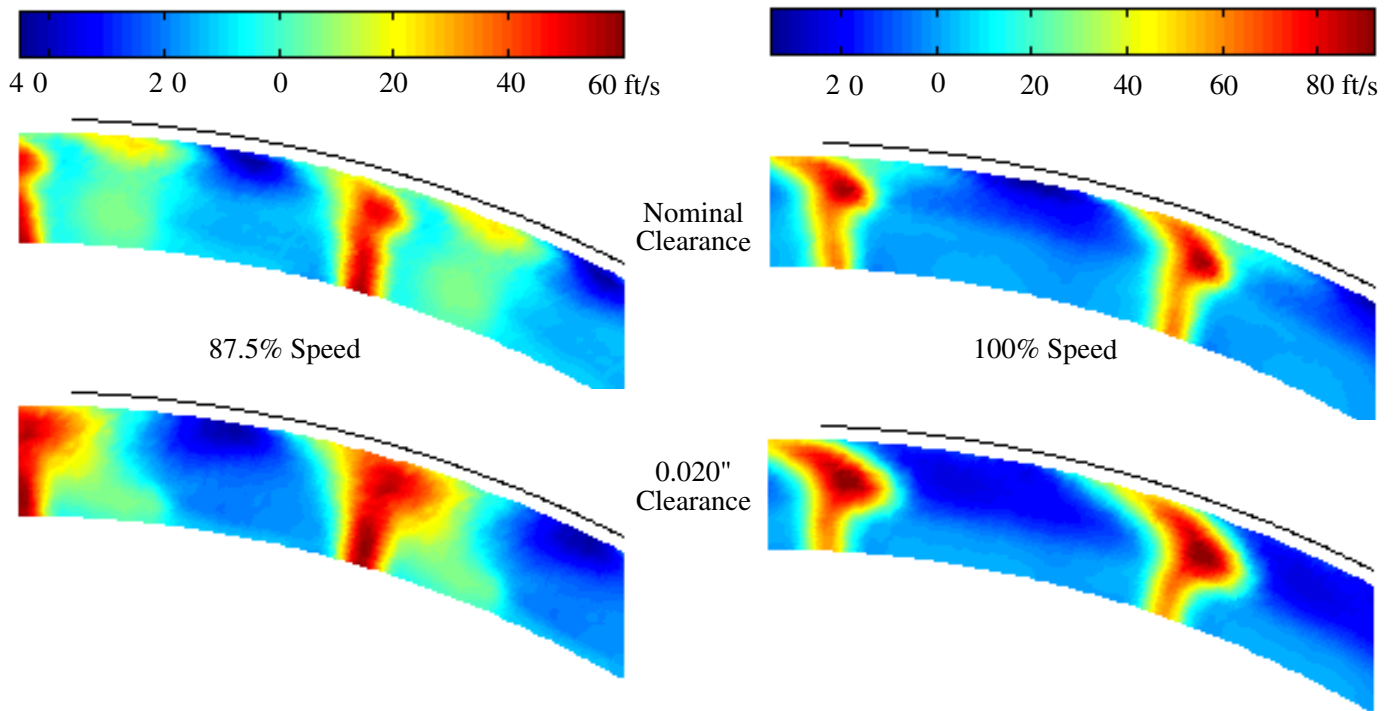
Figure 21. Difference between average passage tangential mean velocities and circumferentially-averaged tangential mean velocities measured downstream of the R4 rotor at axial station LDV1 at two blade tip clearances and two rotor speeds.
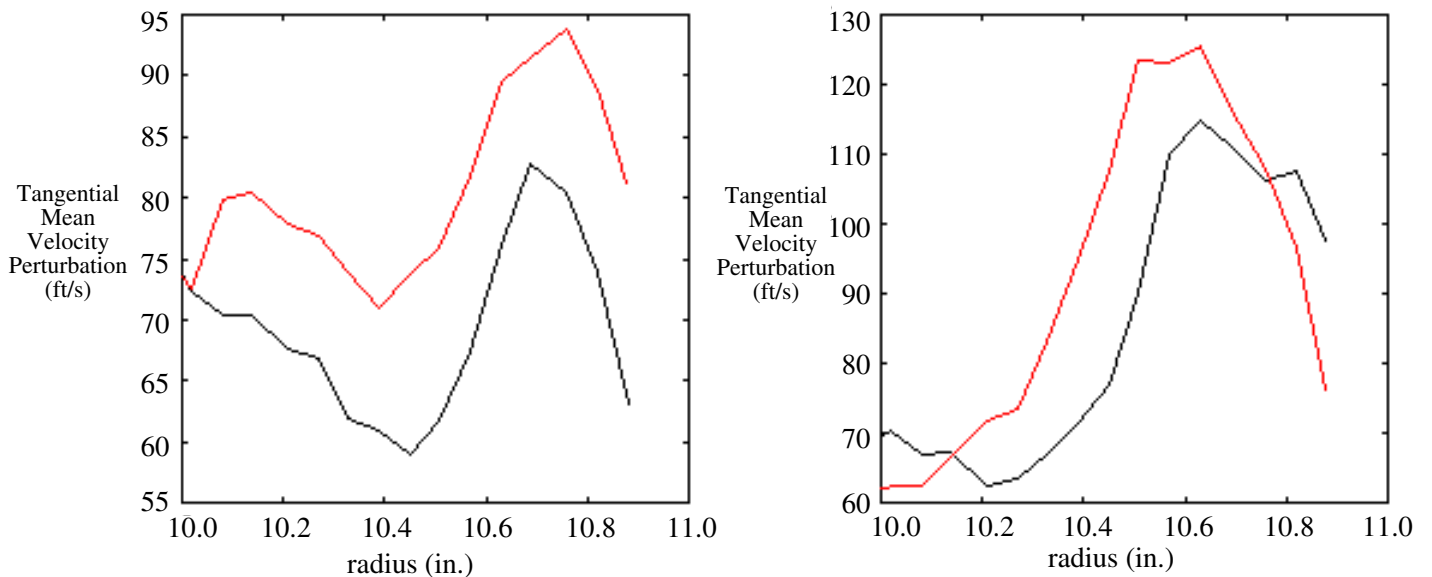

Figure 22. Tangential mean velocity perturbations measured downstream of the tips of the R4 rotor blade with the nominal (shown in black) and 0.020" (red) clearance rubstrips installed in the fan case. Left plot shows perturbations measured at 87.5% speed; right plot shows 100% speed data.
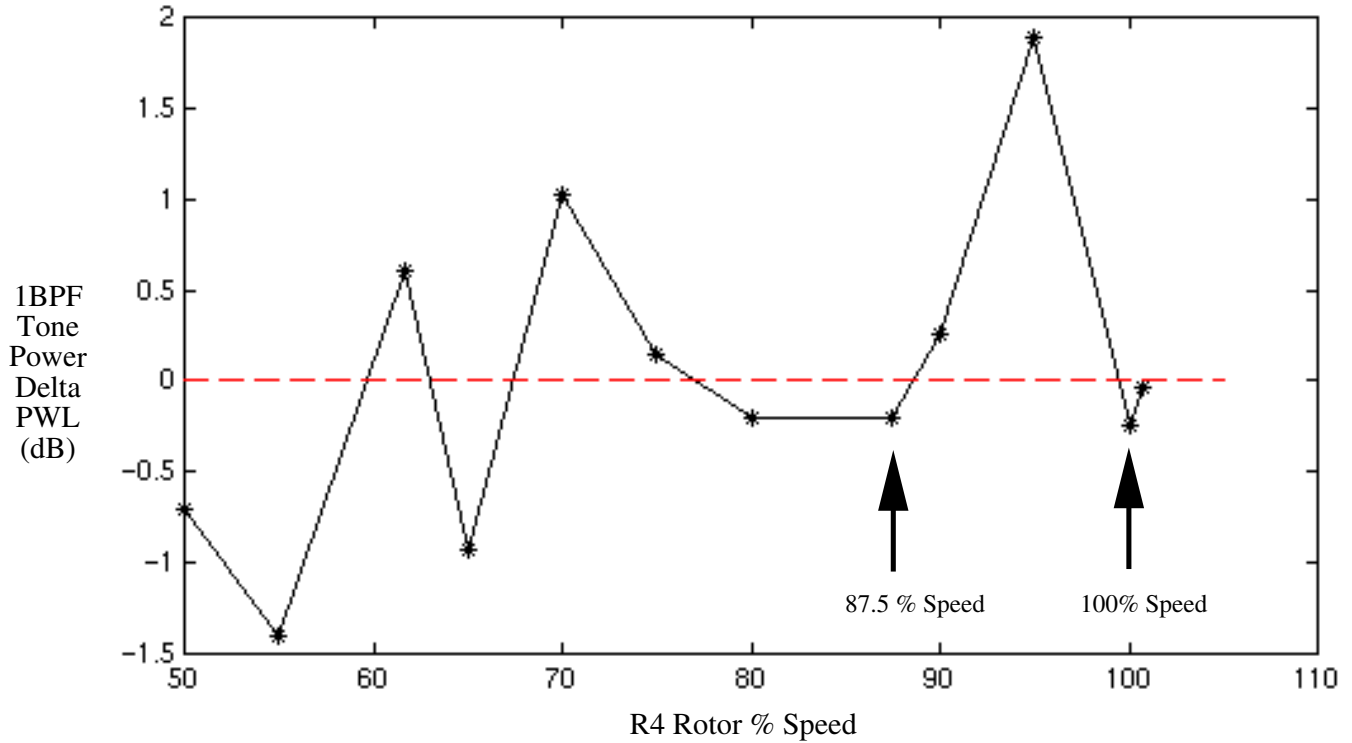
Figure 23. Difference in 1BPF tone power levels measured with 0.020" and nominal clearance rubstrips installed as a function of R4 rotor % design speed. The tone power levels were measured during acoustic runs in which the barrier wall was not installed next to the model. Thus, the tone levels represent the total noise generated (not just that due to rotor/stator interaction.)
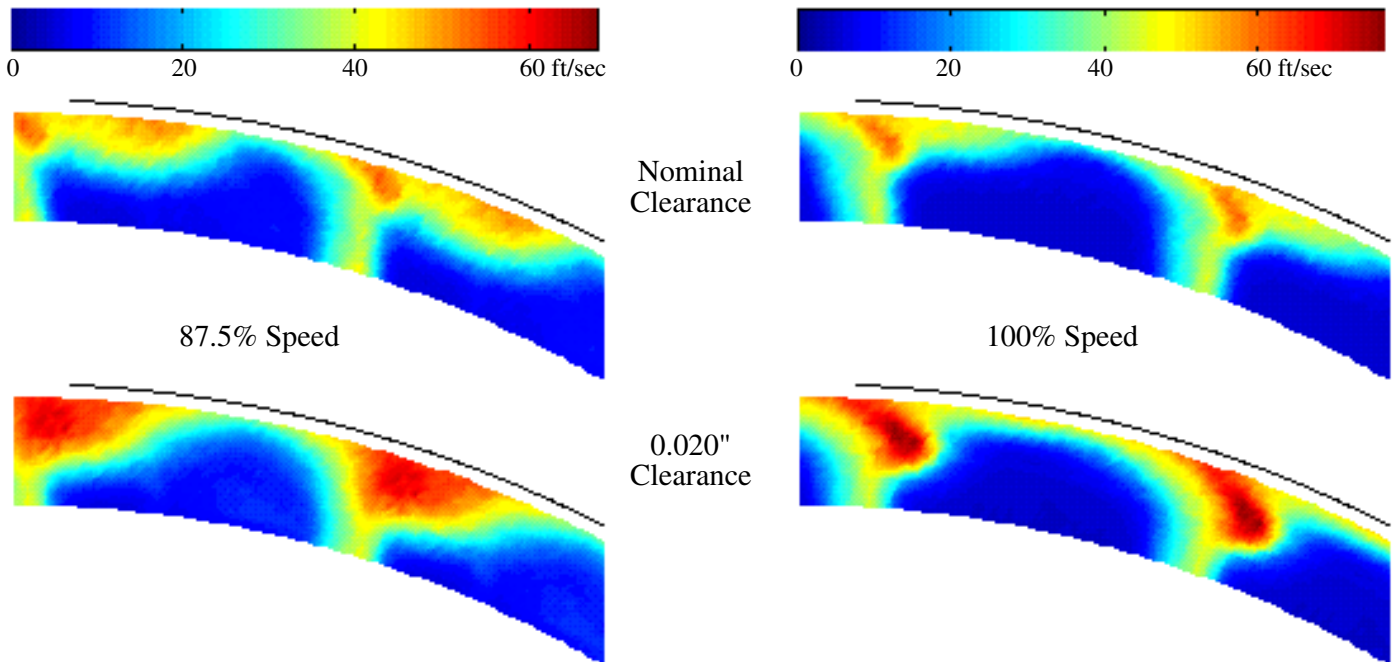

Figure 24. Contours of average passage tangential turbulent velocity showing the tip flow measured downstream of the R4 rotor at axial station LDV1 at two blade tip clearances and two rotor speeds.

REPORT DOCUMENTATION PAGE

Public reporting burden for this collection of information is estimated to average 1 hour per response, including the time for reviewing instructions, searching existing data sources, gathering and maintaining the data needed, and completing and reviewing the collection of information. Send comments regarding this burden estimate or any other aspect of this collection of information, including suggestions for reducing this burden, to Washington Headquarters Services, Directorate for Information Operations and Reports, 1215 Jefferson Davis Highway, Suite 1204, Arlington, VA 22202-4302, and to the Office of Management and Budget, Paperwork Reduction Project (0704-0188), Washington, DC 20503.

1. AGENCY USE ONLY (Leave blank)	2. REPORT DATE	3. REPORT TYPE AND DATES COVERED
	July 2003	Technical Memorandum

4. TITLE AND SUBTITLE

Fan Noise Source Diagnostic Test—LDV Measured Flow Field Results

5. FUNDING NUMBERS

WBS–22–781–30–08

6. AUTHOR(S)

Gary G. Podboy, Martin J. Krupar, Christopher E. Hughes,
and Richard P. Woodward

7. PERFORMING ORGANIZATION NAME(S) AND ADDRESS(ES)

National Aeronautics and Space Administration
John H. Glenn Research Center at Lewis Field
Cleveland, Ohio 44135–3191

8. PERFORMING ORGANIZATION REPORT NUMBER

E–13925

9. SPONSORING/MONITORING AGENCY NAME(S) AND ADDRESS(ES)

National Aeronautics and Space Administration
Washington, DC 20546–0001

10. SPONSORING/MONITORING AGENCY REPORT NUMBER

NASA TM—2003-212330
AIAA–2002–2431

11. SUPPLEMENTARY NOTES

Prepared for the Eighth Aeroacoustics Conference cosponsored by the American Institute of Aeronautics and Astronautics and the Confederation of European Aerospace Societies, Breckenridge, Colorado, June 17–19, 2002. Responsible person, Gary G. Podboy, organization code 5940, 216–433–3916.

12a. DISTRIBUTION/AVAILABILITY STATEMENT

Unclassified - Unlimited
Subject Category: 01   Distribution: Nonstandard

Available electronically at http://gltrs.grc.nasa.gov

This publication is available from the NASA Center for AeroSpace Information, 301–621–0390.

12b. DISTRIBUTION CODE

13. ABSTRACT (Maximum 200 words)

Results are presented of an experiment conducted to investigate potential sources of noise in the flow developed by two 22-in. diameter turbofan models. The R4 and M5 rotors that were tested were designed to operate at nominal take-off speeds of 12,657 and 14,064 RPMC, respectively. Both fans were tested with a common set of swept stators installed downstream of the rotors. Detailed measurements of the flows generated by the two were made using a laser Doppler velocimeter system. The wake flows generated by the two rotors are illustrated through a series of contour plots. These show that the two wake flows are quite different, especially in the tip region. These data are used to explain some of the differences in the rotor/stator interaction noise generated by the two fan stages. In addition to these wake data, measurements were also made in the R4 rotor blade passages. These results illustrate the tip flow development within the blade passages, its migration downstream, and (at high rotor speeds) its merging with the blade wake of the adjacent (following) blade. Data also depict the variation of this tip flow with tip clearance. Data obtained within the rotor blade passages at high rotational speeds illustrate the variation of the mean shock position across the different blade passages.

14. SUBJECT TERMS

Aeroacoustics; Fan noise; Tone noise; Broadband noise; Rotor/stator interaction noise; Laser velocimetry

15. NUMBER OF PAGES

34

16. PRICE CODE

17. SECURITY CLASSIFICATION OF REPORT	18. SECURITY CLASSIFICATION OF THIS PAGE	19. SECURITY CLASSIFICATION OF ABSTRACT	20. LIMITATION OF ABSTRACT
Unclassified	Unclassified	Unclassified	

NSN 7540-01-280-5500

Standard Form 298 (Rev. 2-89)
Prescribed by ANSI Std. Z39-18
298-102